

Article

MHD Williamson Nanofluid Fluid Flow and Heat Transfer Past a Non-Linear Stretching Sheet Implanted in a Porous Medium: Effects of Heat Generation and Viscous Dissipation

Amir Abbas ^{1,*}, Mdi Begum Jeelani ², Abeer S. Alnahdi ^{2,*} and Asifa Ilyas ³

¹ Department of Mathematics, Faculty of Science, University of Gujrat, Sub-Campus Mandi Bahauddin, Mandi Bahauddin 50400, Pakistan

² Department of Mathematics and Statistics, College of Science, Imam Mohammad Ibn Saud Islamic University, Riyadh 13314, Saudi Arabia; mbshaikh@imamu.edu.sa

³ Department of Mathematics, Faculty of Science, University of Sargodha, Sargodha 40100, Pakistan; asifa.ilyas@uos.edu.pk

* Correspondence: cfdamirabbas4693@gmail.com (A.A.); asalnahdi@imamu.edu.sa (A.S.A.)

Abstract: The present study is carried out to examine the behavior of magnetohydrodynamic Williamson nanofluid flow and heat transfer over a non-linear stretching sheet embedded in a porous medium. In the current work, the influence of heat generation and viscous dissipation has been taken into account. The considered phenomenon in the form of partial differential equations is transformed into ordinary differential equations by utilizing an appropriate similarity transformation. The reduced form is solved by using rigorous MATLAB built-in solver bvp4c. The numerical solutions for the velocity field, temperature field, and mass concentration along with the skin friction coefficient, Nusselt number, and Sherwood number are computed. The obtained solutions are shown in graphs and are discussed with physical reasoning. It is noted that by increasing Williamson fluid parameter W , the velocity decreases and concentration profile increases. It is deduced that increasing Eckert number Ec leads to a rise in temperature and mass concentration. It has been viewed that with the increment in heat generation parameter Q , the temperature field increases and concentration decreases. The results show that an increasing magnetic field parameter M leaves a decreasing trend in the velocity field and an increasing trend in the temperature field and concentration profile. The present results are compared with the existing solution which shows good agreement and endorses the validation of current solutions.

Keywords: Williamson fluid; nanofluid; heat transfer; stretching surface; porous medium; heat generation; viscous dissipation



Citation: Abbas, A.; Jeelani, M.B.; Alnahdi, A.S.; Ilyas, A. MHD Williamson Nanofluid Fluid Flow and Heat Transfer Past a Non-Linear Stretching Sheet Implanted in a Porous Medium: Effects of Heat Generation and Viscous Dissipation. *Processes* **2022**, *10*, 1221. <https://doi.org/10.3390/pr10061221>

Academic Editor: Tathagata Acharya

Received: 22 May 2022

Accepted: 15 June 2022

Published: 19 June 2022

Publisher's Note: MDPI stays neutral with regard to jurisdictional claims in published maps and institutional affiliations.



Copyright: © 2022 by the authors. Licensee MDPI, Basel, Switzerland. This article is an open access article distributed under the terms and conditions of the Creative Commons Attribution (CC BY) license (<https://creativecommons.org/licenses/by/4.0/>).

1. Introduction

Efficient ultrahigh cooling systems are an indispensable need for technologies of industries. There are so many limitations of low thermal conductivity when we use ordinary fluids that do not give ultrahigh cooling. Using modern nanotechnology, nanoparticles of metal and nonmetals of the size of a nanometer can be produced and they have versatile thermal, electric, mechanical, magnetic, and fiber characteristics. Nanofluids are made by suspending the nanosized particles in traditional fluids like water, ethylene, and oil. Carbides, carbon nanotubes, oxides, and metals are used to make nanoparticles. The major aim of the development of nanofluids is to obtain the maximum thermal conductivity of a small concentration of nanoparticles through the uniform distribution and stable suspension of nanoparticles in the base fluids. The earliest investigations concerning the variation of thermal conductivity were performed by Masuda et al. [1]. They used ultrafine particles, Al_2O_3 , SiO_2 , and TiO_2 , in water that was used as a base fluid to observe the thermal performance of the fluid. Choi [2], for the first time, introduced the term

nanofluid to explain this new type of nanotechnology-based heat transfer fluids, which have higher thermal conductivities than usual fluids. Experimental investigations in Ref. [3] have been conducted on nanofluids that need only a five-percent volumetric fraction of the nanoparticles for effective heat transfer enhancements, and they used nanofluids as coolants for nuclear powerplants. Buongiorno [4] developed an analytical model for convective transport in nanofluids in which Brownian motion and the thermophoresis effect are taken into account. By this model, the effective heat transfer performance of the fluid can be analyzed theoretically. Sheikholeslami and Sadoughi [5] addressed the nanofluid flow and heat transfer numerically under the melting heat transfer impact with magnetic field influence by using CuO as nanoparticles and water as the base fluid. Abo-Dahab et al. [6] put the light onto the magnetohydrodynamic Casson fluid flow past the non-linear stretching surface that was fixed in a porous medium along with suction/injection effects. They took into account the heat generation and viscous dissipation effects. Shafiq et al. [7] gave an analysis on the stratification effects of Walter's B fluid flow over a Riga surface with radiation impact. Rasool et al. [8] revealed the discussion on the numerical study of magnetohydrodynamic viscoelastic nanofluid flow along the non-linear stretching sheet embedded in a porous medium. They analyzed the influence of Darcy–Forchheimer relation, convective boundary condition, and thermal radiation. Entropy generation magnetohydrodynamic nanofluid flow in squared geometry with Darcy–Forchheimer relation effects was discussed by Fares et al. [9]. Shamshuddin and Mohammad [10] proposed the study of nanofluid flow over a convective elongated surface under the n th order chemical reaction and Joule heating effects.

Non-Newtonian fluid dynamics are one of the most popular research centers of modern machinery due to its promising use in the chemical and food processing industries. Liquids that change the viscosity or flow behavior under pressure are called non-Newtonian fluids. Ramesh et al. [11] studied Williamson fluid over moving and stationary surfaces with convective boundary conditions. The analysis of Williamson fluid flow over a stretching surface has been conducted by Nadeem et al. [12]. The effects of heat transfer on Williamson fluid flow along the porous surface of an exponentially stretching sheet have been explored by Nadeem and Hussain [13]. The peristaltic flow of Williamson fluid under the accomplishment of induced magnetic field through a curved path was explored by Rashid et al. [14]. A non-Newtonian Williamson boundary layer flow was numerically tackled by using a homotopy analysis method by Khan and Khan [15]. The magnetohydrodynamic flow of Williamson fluid with a generalized heat transfer law over a stretching sheet that has variable thickness is dealt numerically by Salahuddin [16]. A non-Newtonian fluid flow model with different flow characteristics and diverse molded conditions has been presented in Refs. [17–20].

Fluid flow in porous media finds significant use in a variety of areas, such as material processing, thermal energy, oil detection, fuel cell technology, flow bed chromatography, etc. The combined effect of heat transfer and temperature across the boundary layer of nanofluid flows through the porous space in the presence of an external magnetic field is considered an effective means of improving thermal performance. A number of research scholars have been engaged in the fluid dynamics of porous media with deferent problems. Vafai and Tien [21] considered the study of solid boundary and inertial forces on fluid flow and heat transfer in a porous medium. Jiang and Ren [22] revealed the study of forced convection in a porous medium employing thermal non-equilibrium model; they included viscous dissipation, variable properties, particles diameter, and thermal dispersion effects. Kothandapani and Srinivas [23] presented magnetohydrodynamic peristaltic transportation and heat transfer under properties of walls action through a porous medium. A discussion on nanofluid flow and convective heat transfer saturated with the porous medium was investigated by Mahdi et al. [24]. Giresha et al. [25] focused their attention on the magnetohydrodynamic boundary layer flow and heat transmission past stretching sheets inserted in a porous medium. Oldroyd-B fluid flow equipped with the Cattaneo–Christov heat flux model under the action of non-linear convection,

Darcy–Forchheimer relation, and variable thermal conductivity was proposed by Shehzad et al. [26]. The investigations concentrating on fluid flows and heat transportation in porous medium are given in Refs. [27–30].

Due to its wide range of applications in various fields of science and industry, fluid flow problems have become one of the most important areas of research today. Other useful uses for this type of investigation include the manufacture of plastic and rubber sheets, the production of glass-fiber, melting spinning, cooling metal plates, etc. Magnetohydrodynamic effects on the three-dimensional flow of nanofluid over a non-linear stretching sheet with non-linear thermal radiation and convective boundary conditions are analyzed numerically by Mahanthesh et al. [31]. Seth et al. [32] carried out the investigations on an unsteady magnetohydrodynamic boundary layer flow of optically dense gray and electrically conducting nanofluid over a non-linear stretching sheet inserted in a porous medium; they encountered the effects of non-linear radiation, convective boundary conditions and entropy generation, and slip velocity. Fluid flows of Newtonian and non-Newtonian fluids and heat transportation processes over a non-linear stretching sheet are presented in Refs. [33–36]. Gorla and Sidawi [37] proposed the mechanism of natural convection along the vertical stretching sheet with the effects of suction and blowing. Megahed [38] gave the numerical analysis of Williamson fluid flow and heat transfer over a non-linear stretching sheet under the action of viscous dissipation and thermal radiation. In Refs. [39–45], the thermo-hydraulic performance of nanofluids theoretically and experimentally through different geometries with diverse flow conditions has been addressed. Avramenko et al. [46] discussed the symmetry of the properties of boundary layer flows by using the Lie group theory technique. Avramenko and Shevchuk [47] proposed the modeling for convective heat and mass transfer in nanofluids with and without boiling and condensation.

In the existing literature, a lot of work on Williamson fluid and nanofluid—separately—was done along the different geometries by taking different fluid characteristics that have been documented due to the physical significance in different areas of sciences. After getting inspiration from the aforementioned fruitful and significant examinations, the present aim is to expose the features of Williamson nanofluid flow over a non-linearly stretching sheet embedded in a porous medium. In the present research work, the external applied magnetic field, heat generation, and viscous dissipation effects on electrically conducting fluid have been incorporated. A thorough review of earlier published works disclose that no such effort has been made before, although the richness of views and the phenomena explained in the present work can be expected to lead to extremely dynamic interactions across disciplines. In the next section, the mathematical procedure, solution procedure, and presentation of results are given.

2. Flow Regime

Consider the steady, viscous, incompressible, and two-dimensional Williamson fluid flow in the region ($y > 0$) past non-linear stretching sheet with a varying velocity distribution $u_w = ax^n$ and wall temperature distribution $T_w = T_\infty + Ax^r$ is considered where $A > 0$, T_∞ is the free stream fluid temperature and C_∞ is the free nanoparticles concentration. The transverse magnetic field with the magnetic field strength $B(x) = B_0x^{\frac{n-1}{2}}$, wherein the electrical field is absent and induced magnetic field is ignored. The coordinates x, y are in the flow direction and normal to the flow direction, respectively. The applied magnetic field, heat generation, and viscous dissipation effects are encountered. The schematic diagram of flow is given in Figure 1. By following Refs. [6,38,46], the governing equations are given below:

$$\frac{\partial u}{\partial x} + \frac{\partial v}{\partial y} = 0 \quad (1)$$

$$u \frac{\partial u}{\partial x} + v \frac{\partial u}{\partial y} = \nu \frac{\partial^2 u}{\partial y^2} + \sqrt{2}\mu\Gamma \frac{\partial u}{\partial y} \frac{\partial^2 u}{\partial y^2} + g\beta_T(T - T_\infty) + g\beta_C(C - C_\infty) - \frac{\sigma}{\rho_f} B^2(x)u - \frac{\nu u}{K^*} \quad (2)$$

$$u \frac{\partial T}{\partial x} + v \frac{\partial T}{\partial y} = \alpha \frac{\partial^2 T}{\partial y^2} + \frac{\nu}{C_p} \left(1 + \frac{\Gamma}{\sqrt{2}} \frac{\partial u}{\partial y} \right) \left(\frac{\partial u}{\partial y} \right)^2 + \frac{Q_0}{\rho C_p} (T - T_\infty) + \tau \left[D_B \left(\frac{\partial T}{\partial y} \frac{\partial C}{\partial y} \right) + \frac{D_T}{T_\infty} \left(\frac{\partial T}{\partial y} \right)^2 \right] \quad (3)$$

$$u \frac{\partial C}{\partial x} + v \frac{\partial C}{\partial y} = D_B \frac{\partial^2 C}{\partial y^2} + \frac{D_T}{T_\infty} \left(\frac{\partial^2 T}{\partial y^2} \right) \quad (4)$$

Flow conditions are,

$$u = u_w(x) = ax^n, v = 0, T = T_w(x) = T_\infty + Ax^r, D_B \left(\frac{\partial C}{\partial y} \right) + \frac{D_T}{T_\infty} \frac{\partial T}{\partial y} = 0 \text{ at } y = 0 \quad (5)$$

$$u \rightarrow 0, T \rightarrow T_\infty, C \rightarrow C_\infty \text{ as } y \rightarrow \infty.$$

where u and v are the velocity components in x and y direction, ρ_f is the density of the fluid, ν is the kinematic viscosity, β_T is the thermal expansion coefficient, α is the thermal diffusivity, C_p is the specific heat, D_T is the thermophoresis coefficient, β_C is the concentration expansion coefficient, Q_0 is the dimensional volumetric heat generation, D_B is the Brownian diffusion coefficient, K^* is the porous medium permeability, and $\tau = \frac{(\rho C)_p}{(\rho C)_f}$ is the effective heat capacity ratio of the nanoparticle material to the effective heat capacity of the fluid. The symbol T_w is wall temperature, T_∞ is ambient temperature, C_w is wall concentration, C_∞ is ambient concentration, n is non-linear stretching sheet index, σ is electrical conductivity, and $B(x) = B_0 x^{\frac{n-1}{2}}$ is the variable magnetic field of strength.

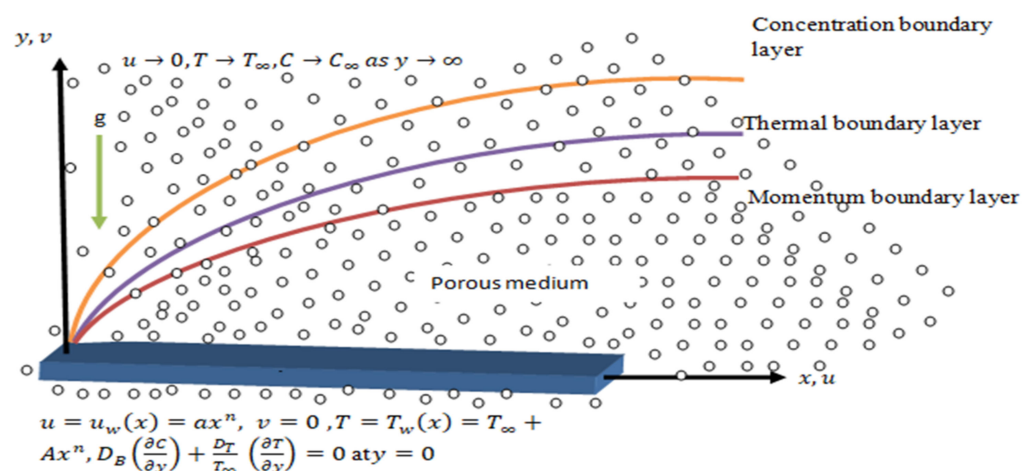


Figure 1. Flow configuration.

Equations (1)–(5) are transformed into ordinary differential equations by employing the following transformation variables:

$$u = ax^n f'(\eta), v = -ax^{n-1} \sqrt{\frac{\nu}{a}} \left(\frac{n+1}{2} f(\eta) + \frac{n-1}{2} \eta f'(\eta) \right), \eta = \sqrt{\frac{\nu}{a}} x^{\frac{n-1}{2}} y, \quad (6)$$

$$\theta = \frac{T - T_\infty}{T_\infty - T_w}, \phi = \frac{C - C_\infty}{C - C_w}$$

By utilizing Equation (6) in Equations (1)–(5), we have the following transformed equations:

$$f''' + \frac{n+1}{2} f f'' - n f'^2 + W f''' f'' - M f' - K f' + \lambda_T \theta + \lambda_C \phi \quad (7)$$

$$\frac{1}{Pr} \theta'' + \frac{n+1}{2} f \theta' - n f' \theta + Q \theta + Nb \theta' \phi' + Nt \theta'^2 + Ec \left(1 + \frac{W}{2} f'' \right) f''^2 \quad (8)$$

$$\frac{1}{Sc}\phi'' + \frac{n+1}{2}f\phi' + \frac{Nb}{Nt}\theta'' = 0 \quad (9)$$

Subjected boundary conditions

$$\begin{aligned} f = 0, f' = 1, \theta = 1, Nb\phi' + Nt\theta' = 0 \text{ at } \eta = 0 \\ f' \rightarrow 0, \theta \rightarrow 0, \phi \rightarrow 0 \text{ as } \eta \rightarrow \infty \end{aligned} \quad (10)$$

The parameters appearing in Equations (7)–(10) are defined as the Prandtl number $Pr = \frac{\nu}{\alpha}$, Schmidt number $Sc = \frac{\nu}{D_B}$, thermophoresis parameter $Nt = \frac{(\rho C)_p D_T (T_w - T_\infty)}{(\rho C)_f T_\infty \nu}$, mixed convection parameter $\lambda_T = \frac{Gr_T}{Re^2}$, magnetic field parameter $M = \frac{\sigma B_0^2}{\rho_f a}$, porous medium parameter $K = \frac{\nu}{aK^*}$, Eckert number $Ec = \frac{u_w^2}{C_p(T_w - T_\infty)} = \frac{a^2 x^{2n-r}}{AC_p}$, Williamson parameter $W = \sqrt{2} \frac{x^{\frac{3n-1}{2}} a^{\frac{3}{2}} \Gamma}{\nu^{1/2}}$, a non-linear stretching index n , and r is a constant. Also, there is the Brownian motion parameter $Nb = \frac{(\rho C)_p D_B (C_w - C_\infty)}{(\rho C)_f \nu}$, heat generation parameter $Q = \frac{Q_0}{u_w \rho C_p}$, and modified mixed convection parameter $\lambda_C = \frac{Gr_C}{Re^2}$. After analyzing, we observed that both the W and Ec parameters are functions of x . To overcome this situation that gives a non-similar solution for our present problem, we should take $r = 2n = 2/3$. Given this, these parameters take the form $W = \frac{\sqrt{2} a^{\frac{3}{2}} \Gamma}{\sqrt{\nu}}$, which is the Williamson fluid parameter, and $Ec = \frac{u_w}{C_p(T_w - T_\infty)} = \frac{a^2}{AC_p}$, which is the Eckert number. This assumption ensures a similar solution to the current problem.

The quantities of practical interest in this study are the skin friction coefficient C_f and the Nusselt number Nu and Sherwood number Sh which are defined as:

$$\begin{aligned} C_f = \frac{\tau_w}{\rho u_w^2}, Nu = \frac{xq_w}{k(T_w - T_\infty)}, Sh = \frac{xq_m}{D_B(C_w - C_\infty)}. \\ \text{where } \tau_w = \mu \left(\left(\frac{\partial u}{\partial y} \right) + \frac{\Gamma}{\sqrt{2}} \frac{\partial u}{\partial y} \right) \Big|_{y=0}, q_w = -k \left(\frac{\partial T}{\partial y} \right) \Big|_{y=0}, q_m = -D_B \left(\frac{\partial C}{\partial y} \right) \Big|_{y=0} \end{aligned} \quad (11)$$

By using variables defined in Equation (6), we have the following:

$$Re^{1/2} C_f = f''(0) + \frac{W}{2} f''(0), Re^{-1/2} Nu = -\theta'(0), Re^{-1/2} Sh = -\phi'(0), \quad (12)$$

3. Solution Methodology

The determination of the solution for Equations (7)–(10) is analytically cumbersome, so the numerical evaluation is done for several parameter values, namely the Prandtl number Pr , Schmidt number Sc , thermophoresis parameter Nt , mixed convection parameter λ_T , Magnetic field parameter M , porous medium parameter K , Eckert number Ec , Williamson parameter W , a non-linear stretching index n , Brownian motion parameter Nb , heat generation parameter Q , and modified mixed convection parameter λ_C . A set of solutions for the flow model is computed by employing `bvp4c`, a MATLAB built-in function. An algorithm for this solver utilizes a three-stage Labato formula and has the basis of a finite difference code called the collocation formula. A collocation polynomial is C^1 -continuous and has fourth-order accuracy. To substitute Equations (7)–(10) into this solver's algorithm, first we have to convert them into first-order ordinary differential equations. The current results for f' , θ , and ϕ at $\eta = 3$ (say) are given with boundary conditions $f'(3) = 1$, $\theta(3) = 1$, and $Nb\phi'(3) + Nt\theta'(3) = 0$, then we apply the MATLAB built-in numerical solver `bp4c` with step size $\Delta\eta = 0.1$. By adjusting the η_{max} and $\Delta\eta$, we obtain the converged results within a tolerance limit of 10^{-6} . The computed results satisfy the given boundary conditions asymptotically, which indicates the accuracy of the obtained solutions.

4. Results and Discussion

The current section reveals the physics that occurred in the flow regime for computations of the velocity field $f'(\eta)$, temperature field $\theta(\eta)$, and mass concentration $\phi(\eta)$ for numerous values of flow parameters, which specify the flow features. The skin friction coefficient $Re^{1/2}C_f$, Nusselt number $Re^{-1/2}Nu$, and Sherwood number $Re^{-1/2}Sh$ are also calculated. All of the results are graphed under the flow parameters: Prandtl number Pr , Schmidt number Sc , thermophoresis parameter Nt , mixed convection parameter λ_T , magnetic field parameter M , porous medium parameter K , Eckert number Ec , Williamson parameter W , a non-linear stretching index n , Brownian motion parameter Nb , heat generation parameter Q , and modified mixed convection parameter λ_C .

4.1. Influence of Regulatory Flow Parameters on Velocity Field $f'(\eta)$, Temperature Field $\theta(\eta)$, and Mass Concentration $\phi(\eta)$

Figures 2–4 are sketched for velocity field $f'(\eta)$, temperature field $\theta(\eta)$, and mass concentration $\phi(\eta)$, respectively, against numerous values of λ_T while other parameters values are preset. Graphs reveal that intensification in λ_T lead to increase in $f'(\eta)$ in Figure 2, and decrease in $\theta(\eta)$ and $\phi(\eta)$ in Figures 3 and 4, respectively. The impact of non-linear stretching sheet index n on $f'(\eta)$, $\theta(\eta)$, and $\phi(\eta)$ is displayed in Figures 5–7. Graphical attitude fleshes out that augmentation in n causes to decline $f'(\eta)$, $\theta(\eta)$, and $\phi(\eta)$. An effect of Williamson fluid parameter W on velocity and concentration profiles is shown in Figures 8 and 9. From sketches, W enhancement in $f'(\eta)$ gives a decline in $\phi(\eta)$ and rise to $\theta(\eta)$. As W increases, the viscosity of the fluid is recued so that the nanoparticles move freely and the mass concentration increases rapidly. Influence of porous medium parameter K on already mentioned properties is reported in Figures 10–12. It is viewed that increasing K leaves the decreasing trend in $f'(\eta)$, and increasing trend in $\theta(\eta)$, and increasing trend in $\phi(\eta)$ and in Figures 10–12. As K is increased porosity of the medium decreased and viscous forces are enhanced, due to which temperature and concentration are enhanced. Figures 13 and 14, is due to Pr the cation of $f'(\eta)$ on $\theta(\eta)$, and graphs indicate that increasing Pr reduces the velocity and temperature. This trend, as seen in Figures 13 and 14, is due to fact that an augmentation in Pr is because of an increase in the viscosity and a decrease in thermal conductance, due to which the velocity of the fluid—but not the temperature of the fluid—decline remarkably. The momentum and thermal boundary layer thickness is thickened. Control of thermophoresis parameter Nt on $f'(\eta)$, $\theta(\eta)$, and $\phi(\eta)$ is demonstrated in Figures 15–17, respectively. We can note that rising Nt causes to reduce $f'(\eta)$, $\theta(\eta)$, and $\phi(\eta)$. An action of Brownian motion parameter Nb on fields of velocity, temperature, and concentration is portrayed in Figures 18–20, respectively. Sketches show that as Nb is raised, all $f'(\eta)$, $\theta(\eta)$, and $\phi(\eta)$ get stronger rapidly. The parameter M on $f'(\eta)$, $\theta(\eta)$, and $\phi(\eta)$ are shown in Figures 21–23, respectively. It is noted that for increasing M , a decreasing trend in $f'(\eta)$, and enhancing trend in $\theta(\eta)$, and $\phi(\eta)$ is observed. It is due to the fact that θ is enhanced that a strong Lorentz force is generated that compels the fluid flow to slow down due to the generation of resistance temperature, which is augmented. Physical behavior of θ and ϕ against Ec is portrayed in Figures 24 and 25, respectively. Increasing Ec is leaving the increasing behavior for $\theta(\eta)$, and $\phi(\eta)$. For viscous dissipation thermal energy is converted to mechanical energy. By increasing Ec more forces act to dissipate the viscosity so more work has to be done by the fluid on them due to which temperature of the fluid rise and consequently more mass concentration is noted. Heat generation parameter Q effect on $\theta(\eta)$ and $\phi(\eta)$ is given in Figures 26 and 27, respectively. It is noted that as Q is enhanced $\theta(\eta)$ increase and $\phi(\eta)$ decreases with reasonable difference.

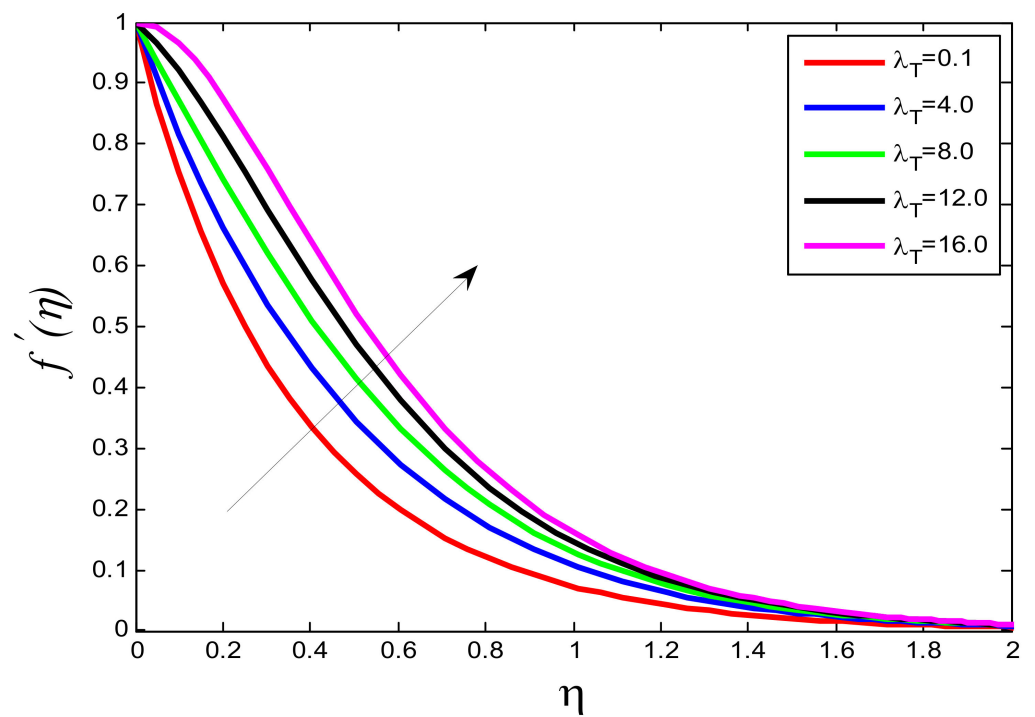


Figure 2. Influence of λ_T on $f'(\eta)$.

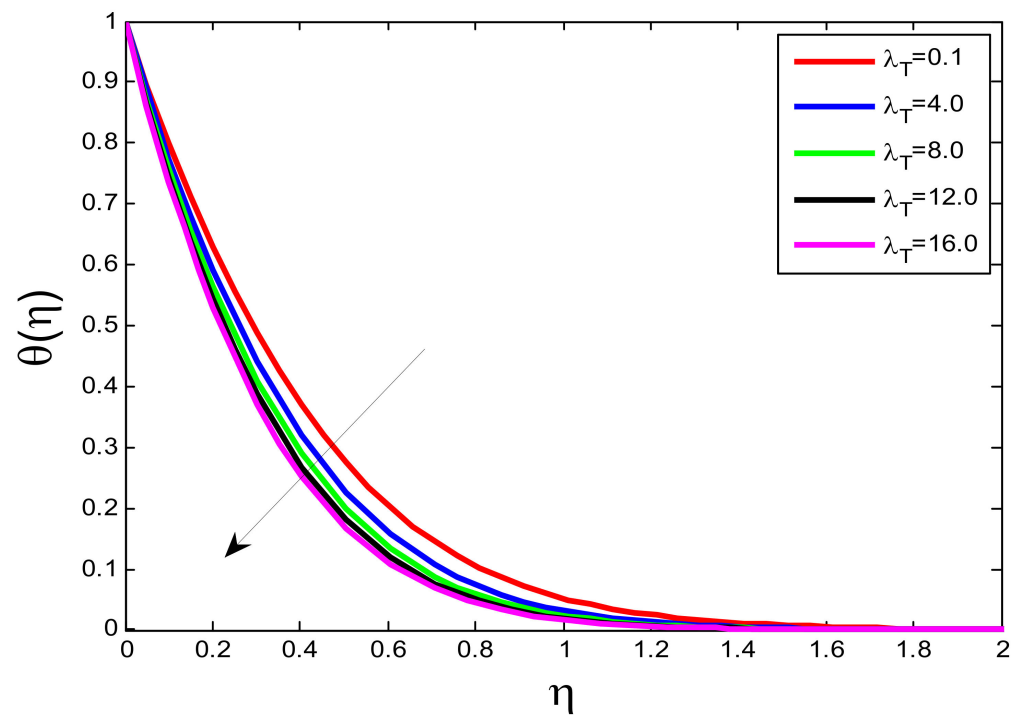


Figure 3. Influence of λ_T on $\theta(\eta)$.

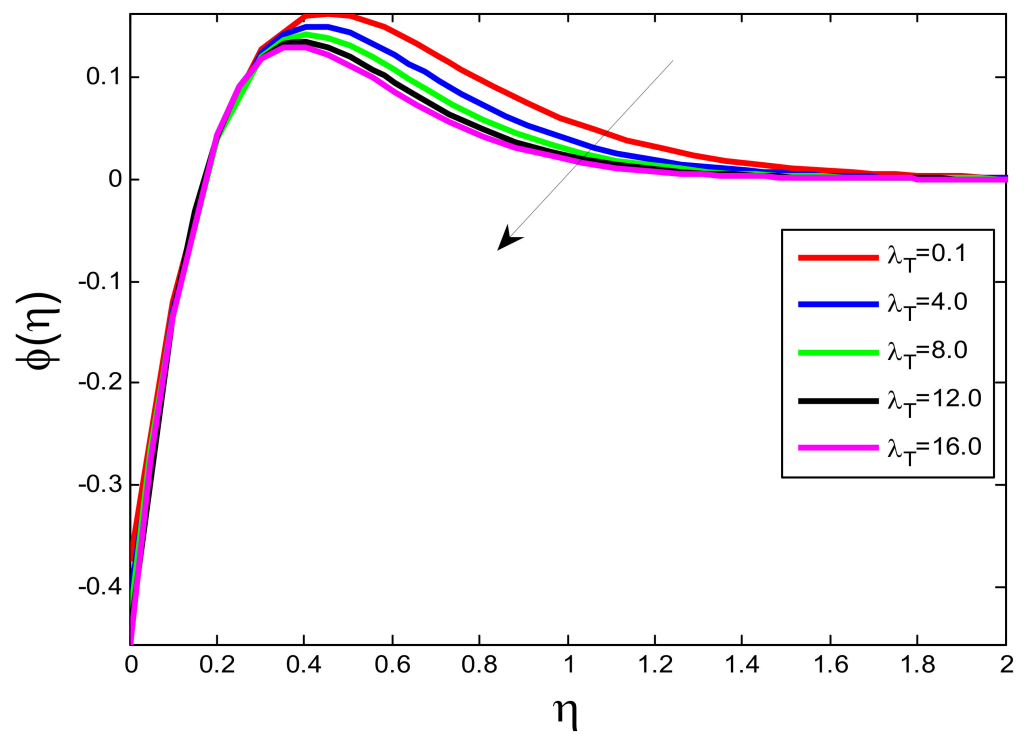


Figure 4. Influence of λ_T on $\phi(\eta)$.

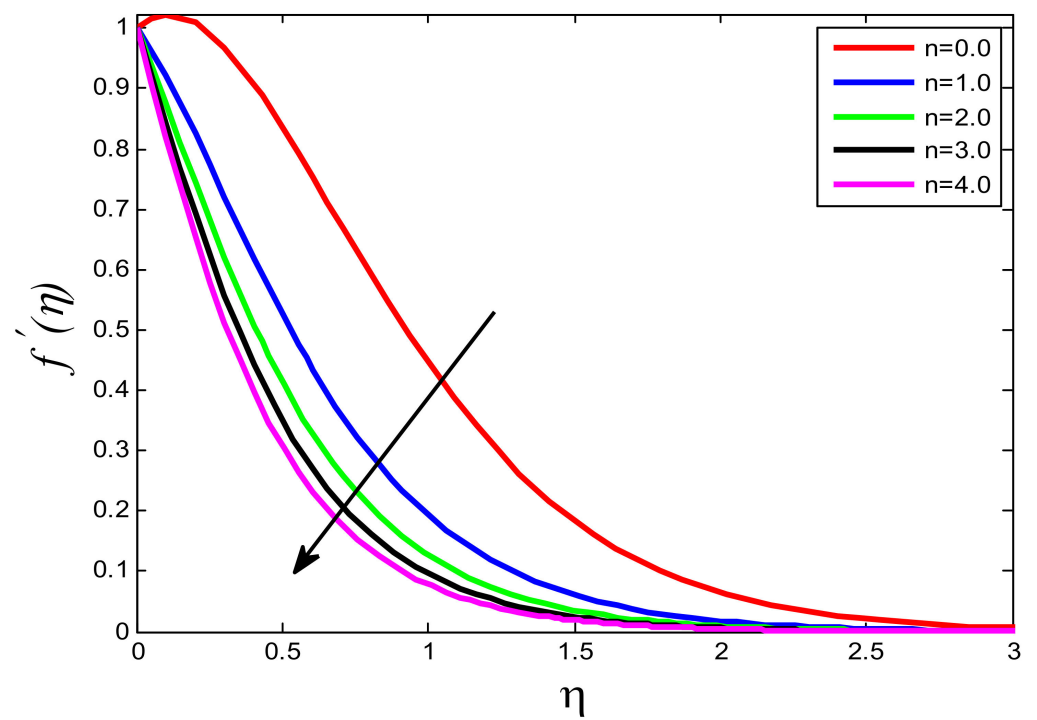


Figure 5. Influence of n on $f'(\eta)$.

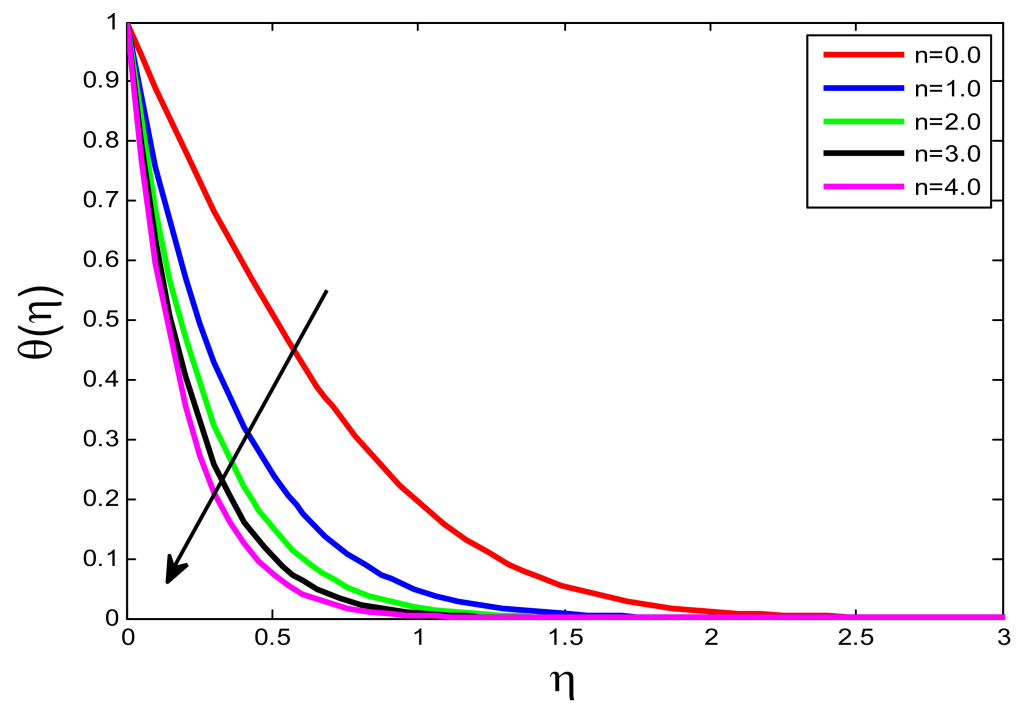


Figure 6. Influence of n on $\theta(\eta)$.

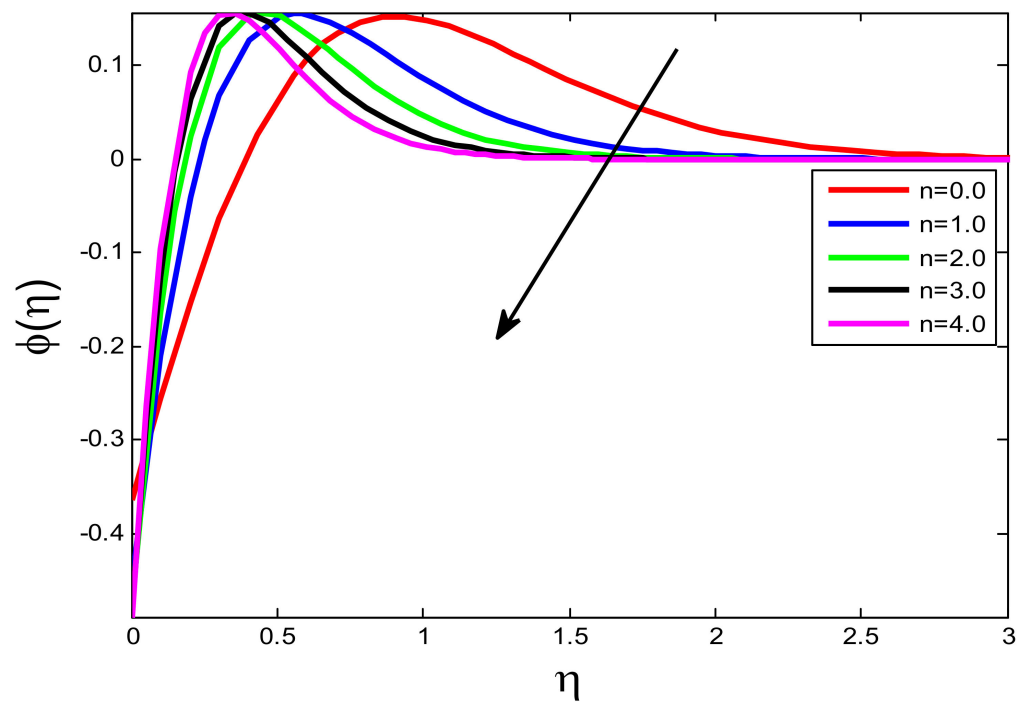


Figure 7. Influence of n on $\phi(\eta)$.

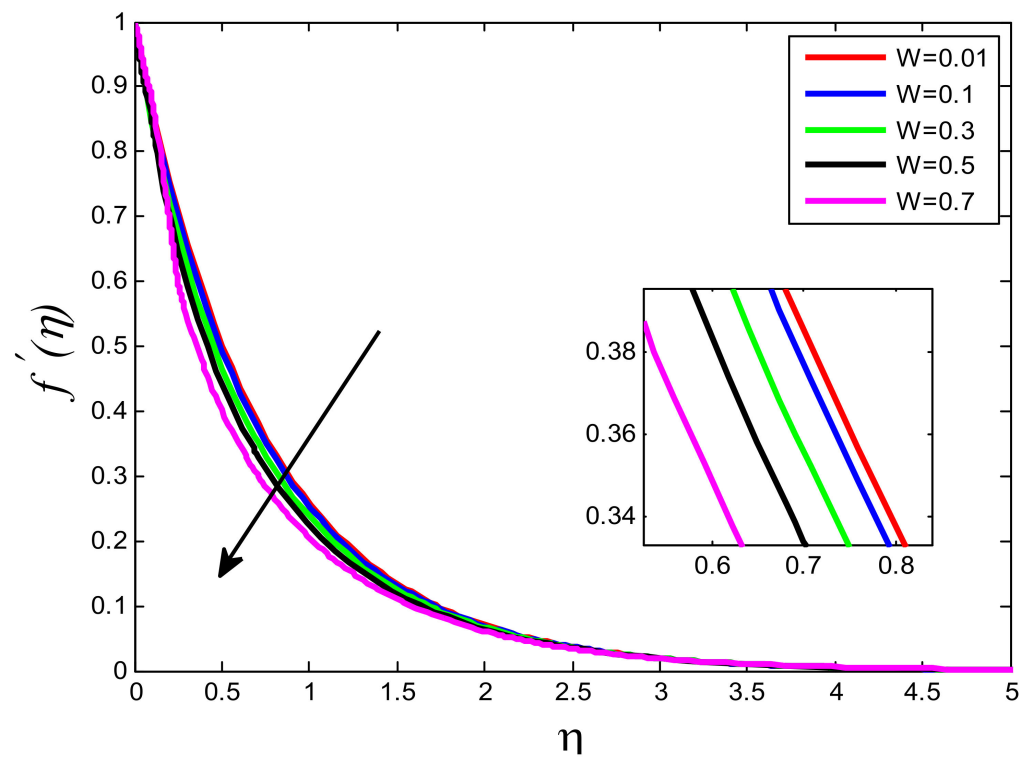


Figure 8. Influence of W on $f'(\eta)$.

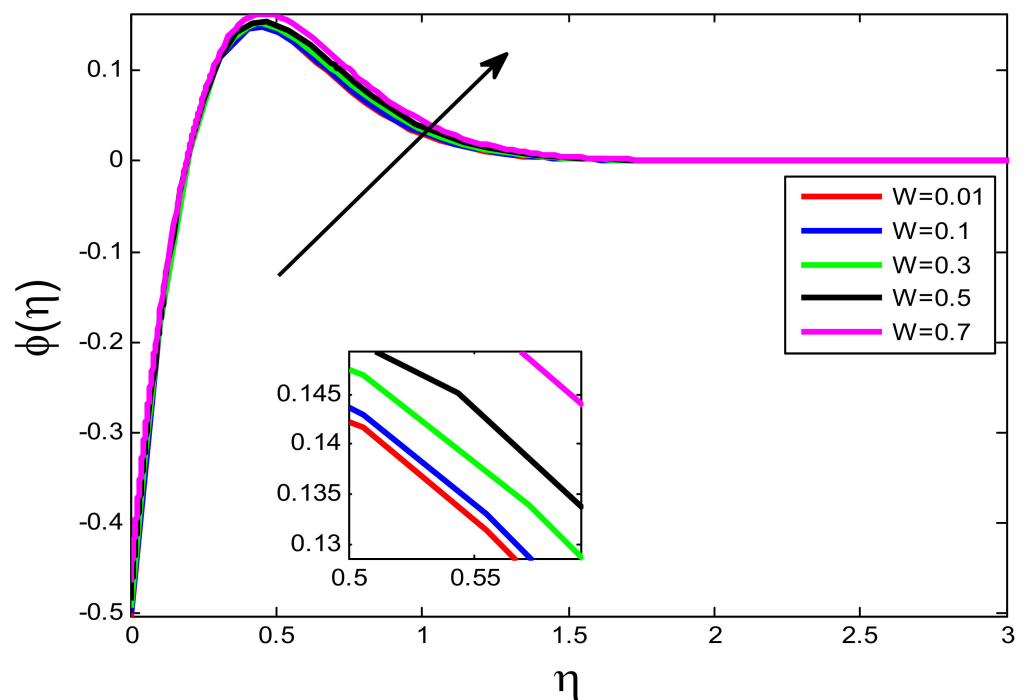


Figure 9. Influence of W on $\phi(\eta)$.

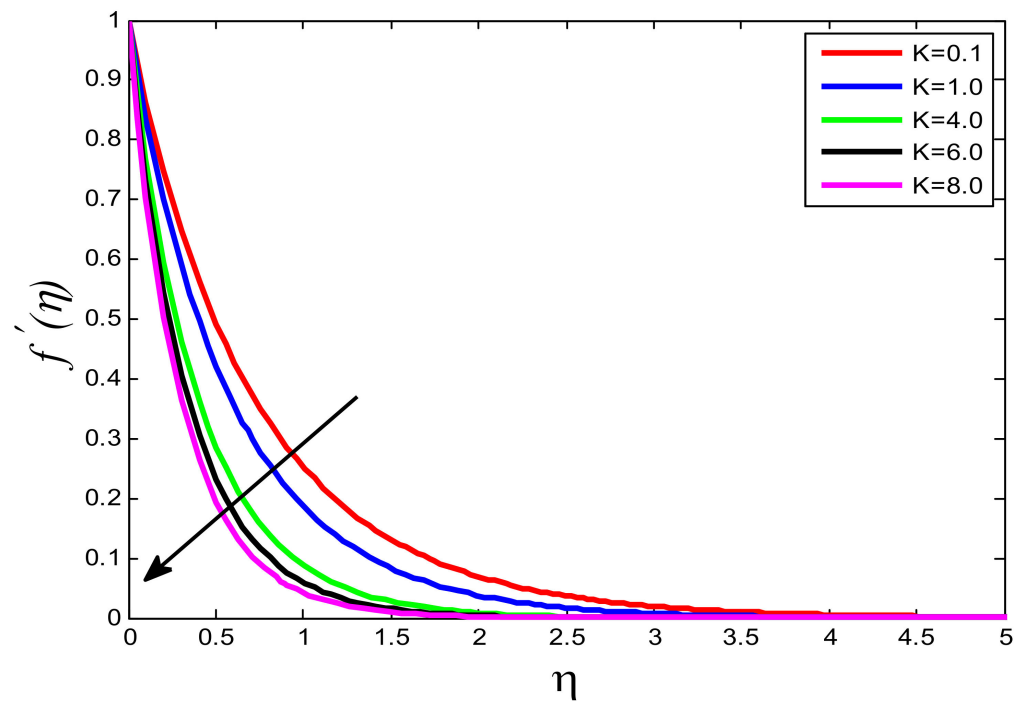


Figure 10. Influence of K on $f'(\eta)$.

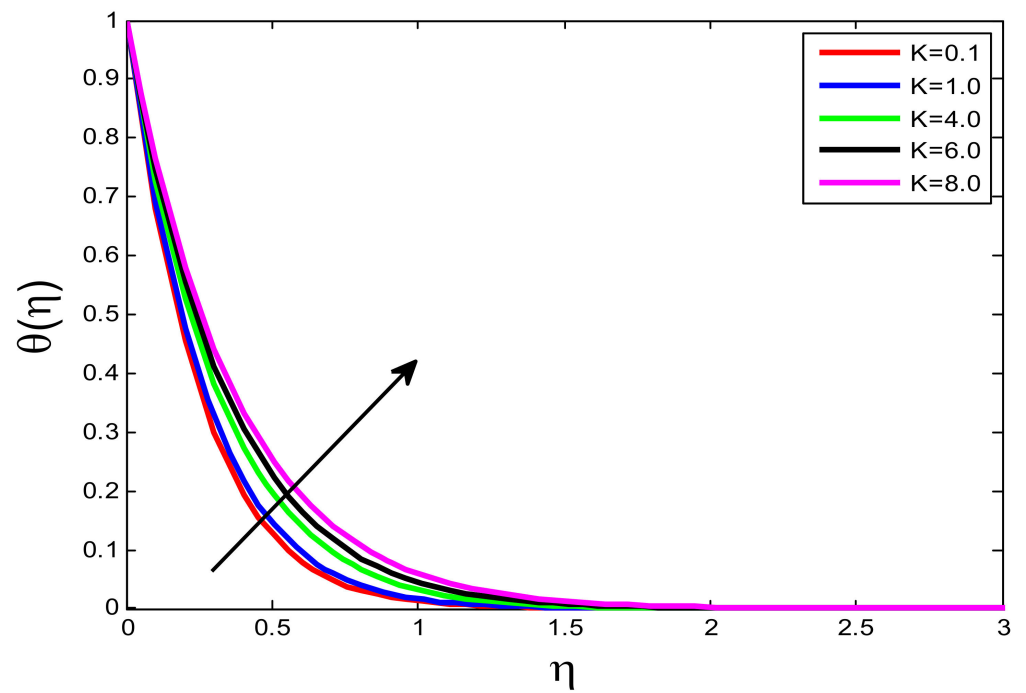


Figure 11. Influence of K on $\theta(\eta)$.

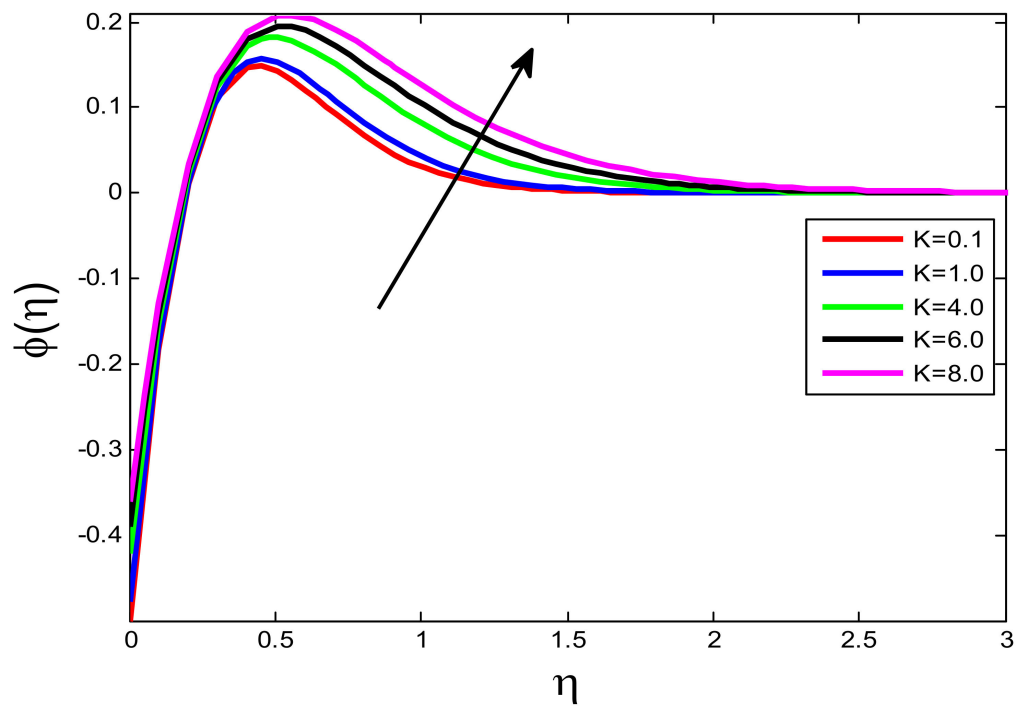


Figure 12. Influence of K on $\phi(\eta)$.

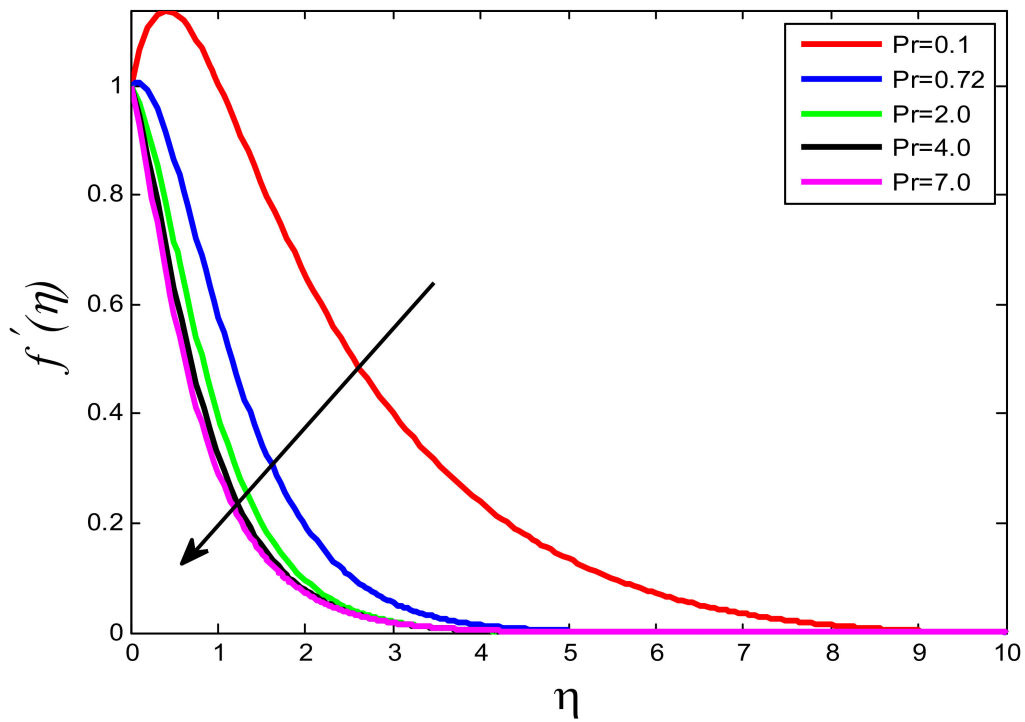


Figure 13. Influence of Pr on $f'(\eta)$.

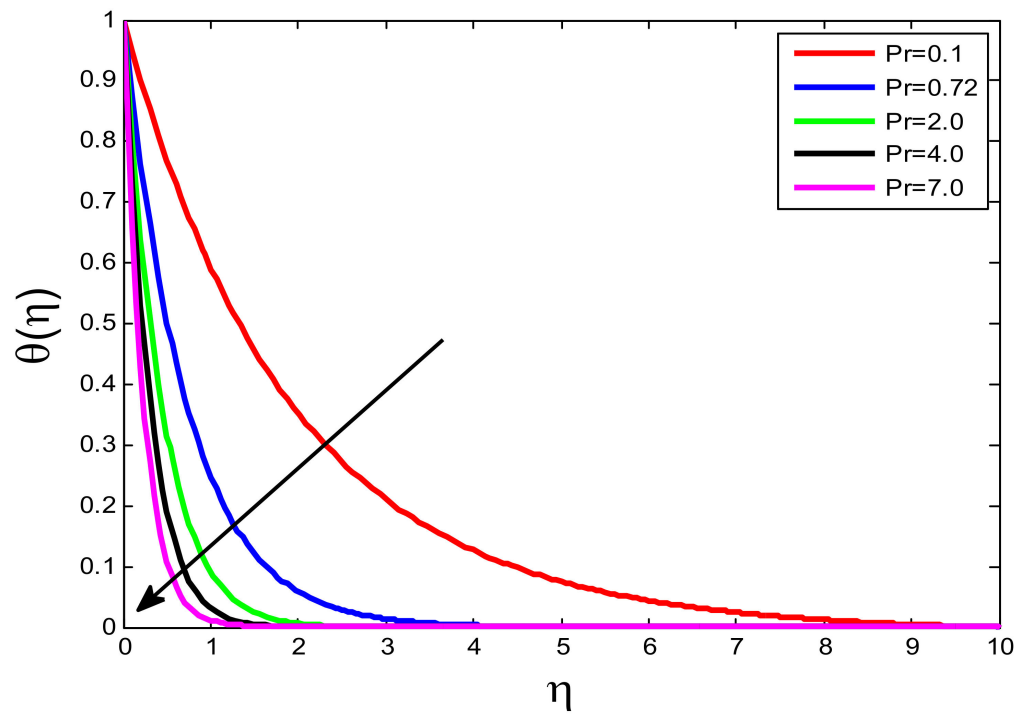


Figure 14. Influence of Pr on $\theta(\eta)$.

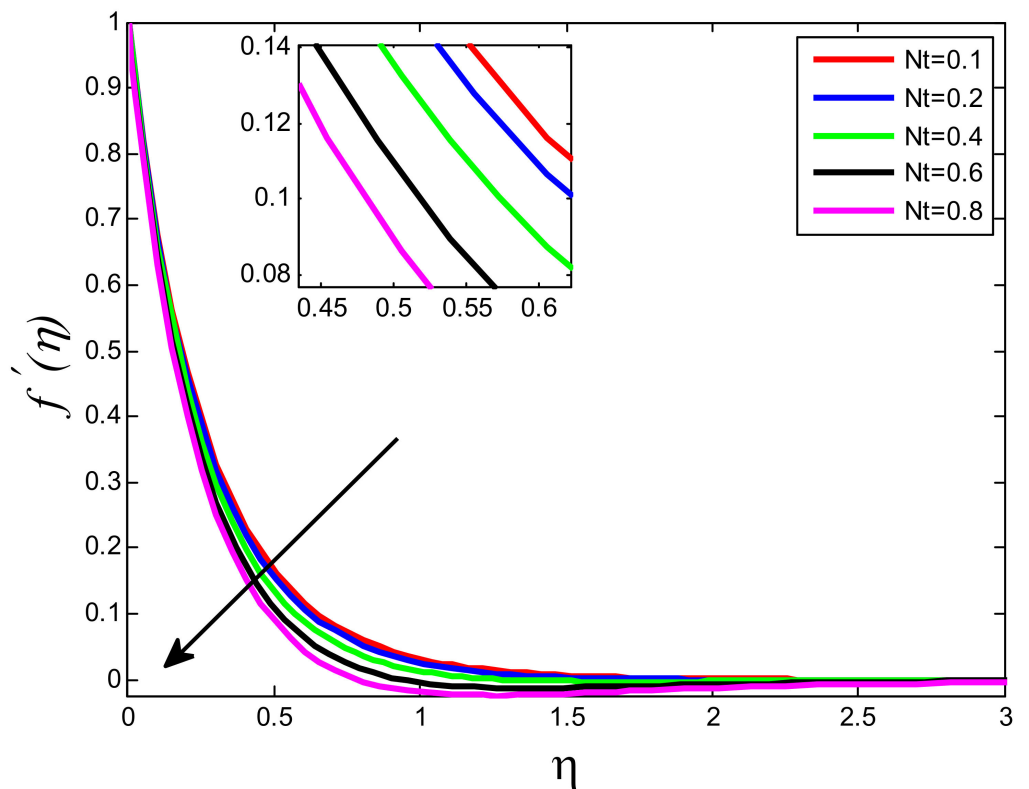


Figure 15. Influence of Nt on $f'(\eta)$.

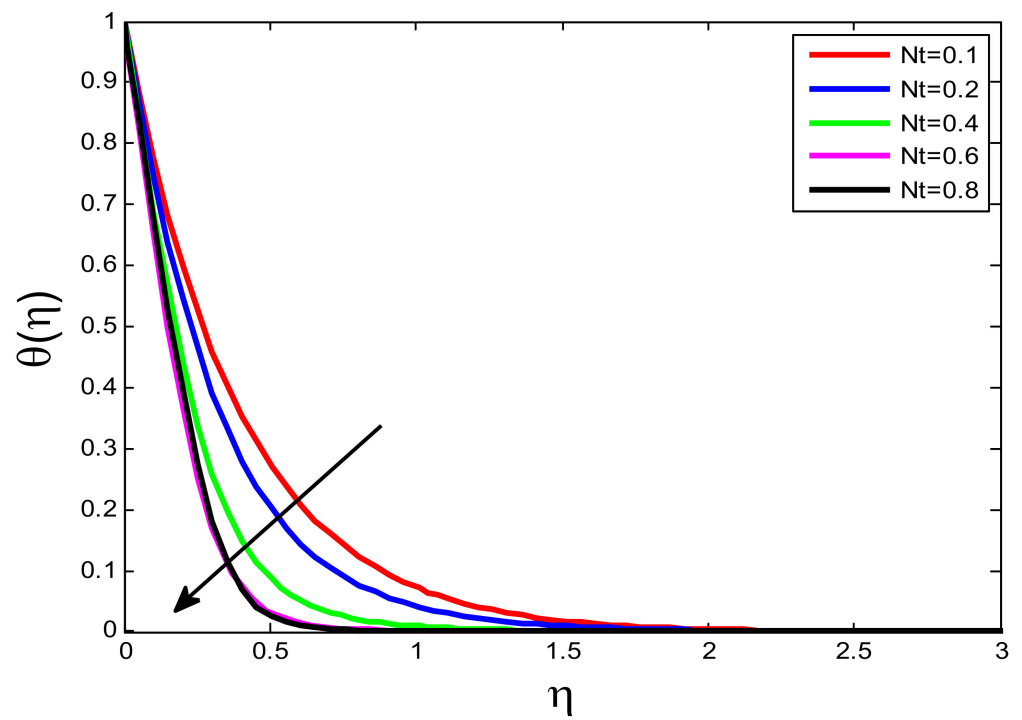


Figure 16. Influence of Nt on $\theta(\eta)$.

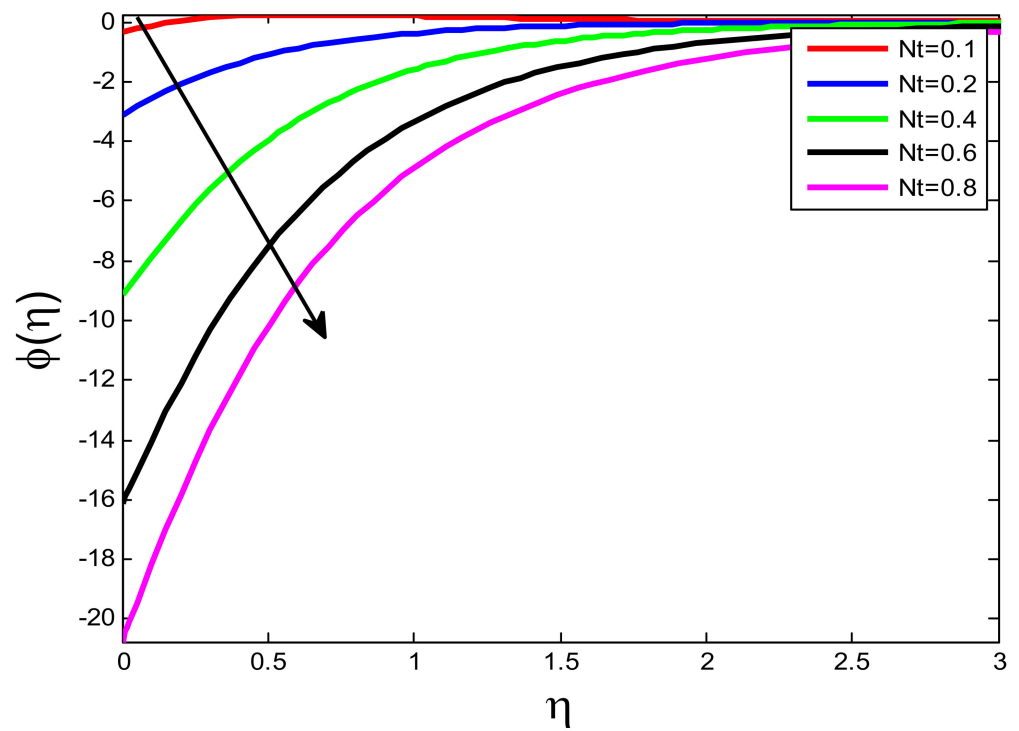


Figure 17. Influence of Nt on $\phi(\eta)$.

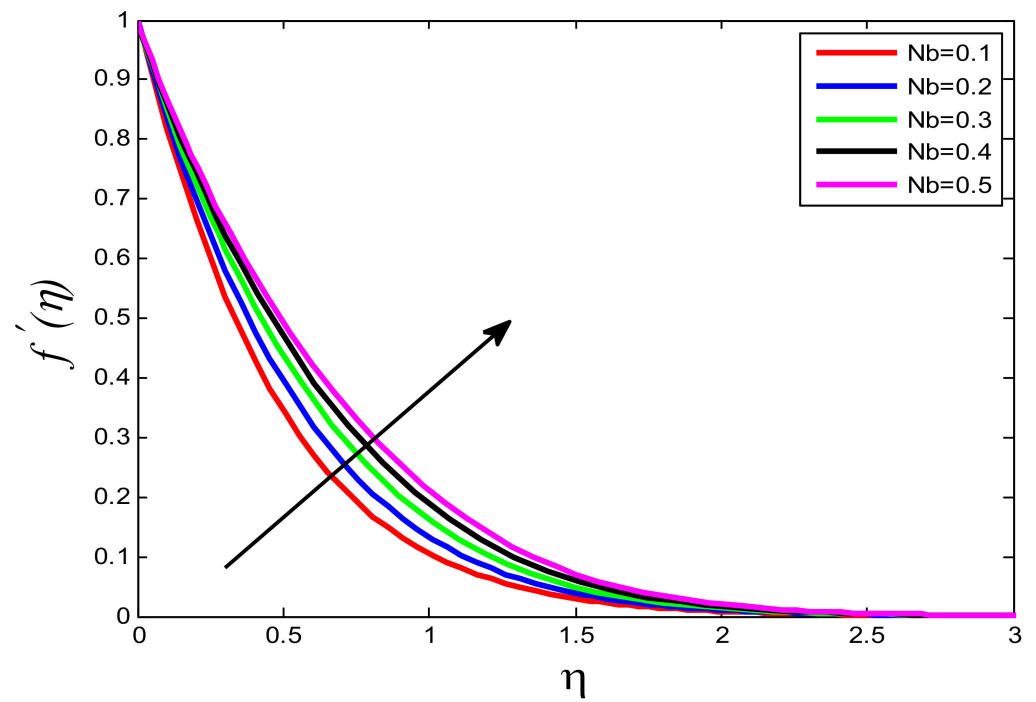


Figure 18. Influence of Nb on $f'(\eta)$.

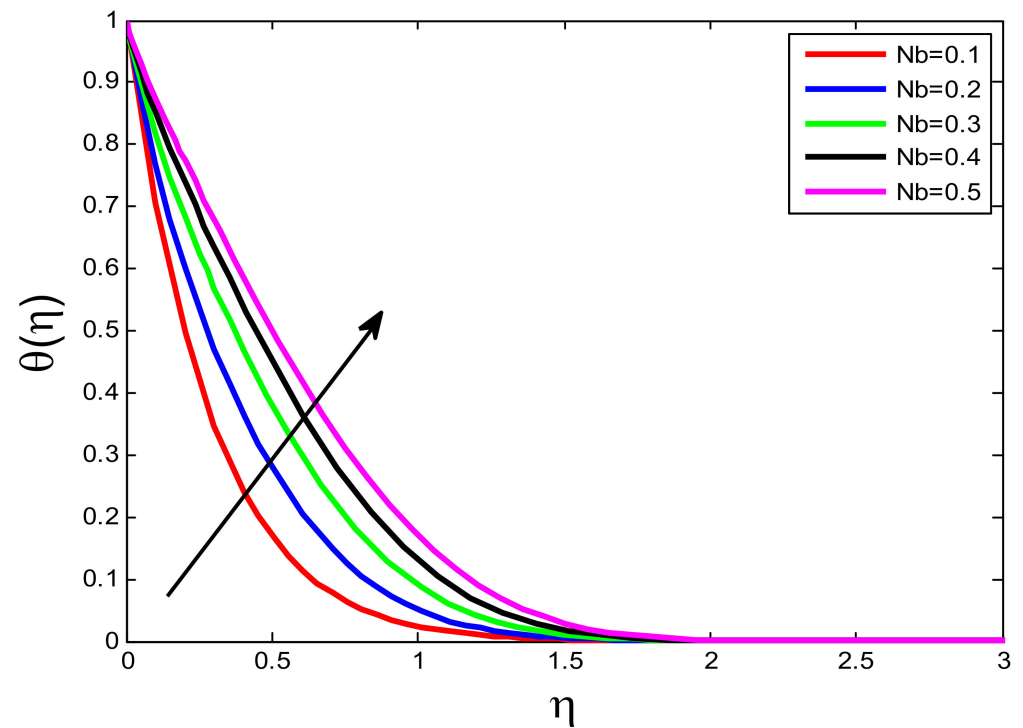


Figure 19. Influence of Nb on $\theta(\eta)$.

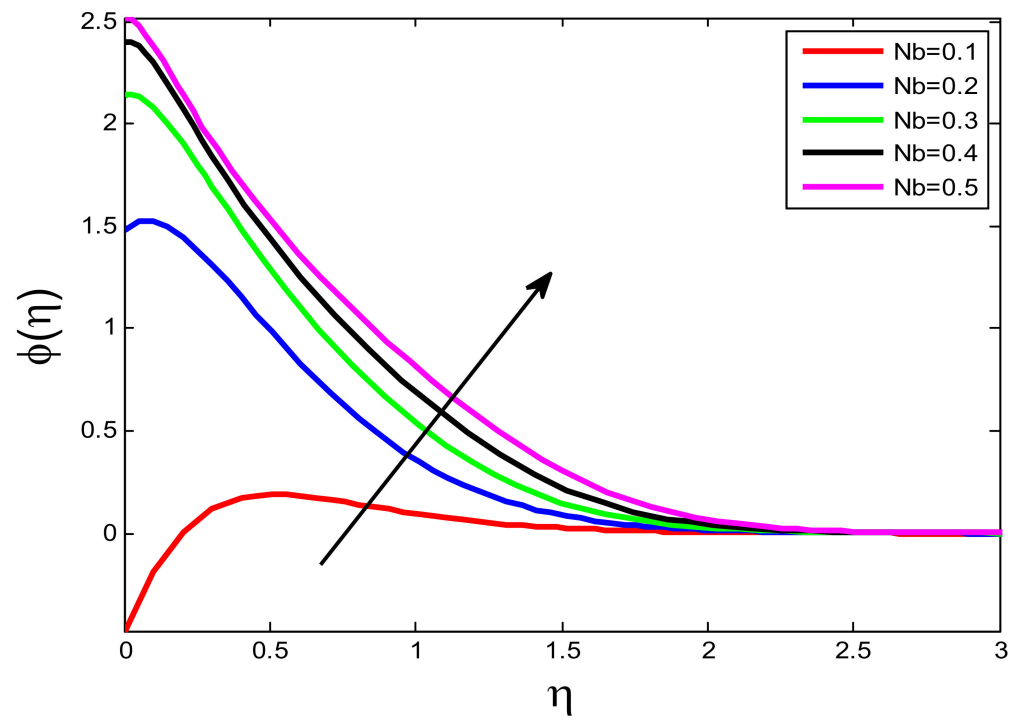


Figure 20. Influence of Nb on $\phi(\eta)$.

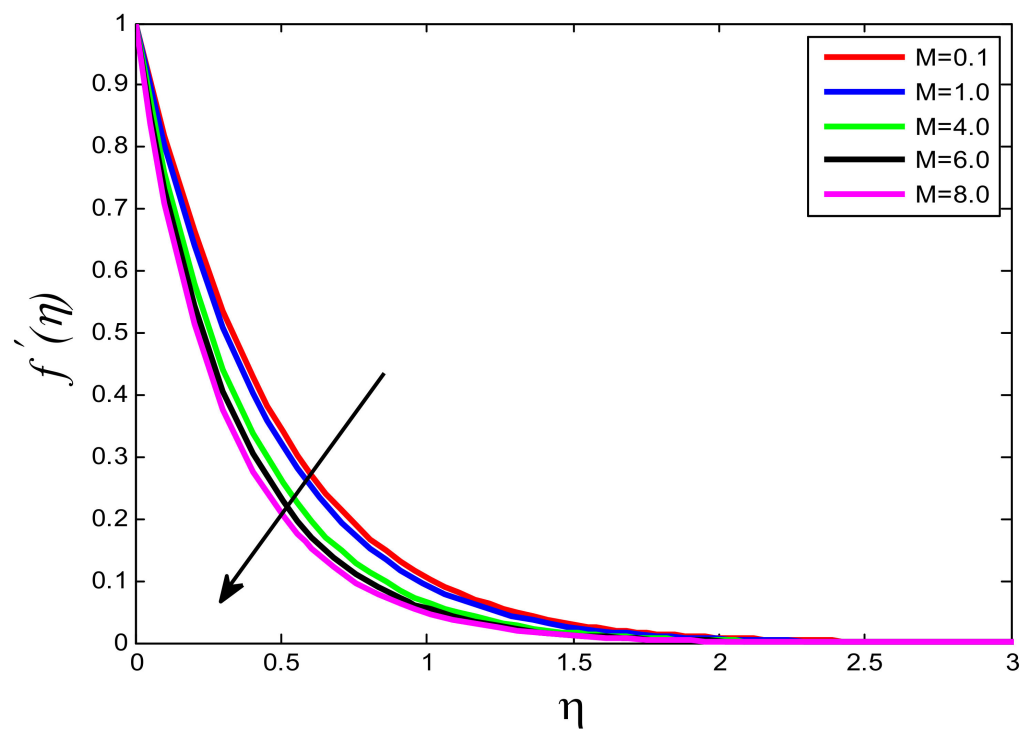


Figure 21. Influence of M on $f'(\eta)$.

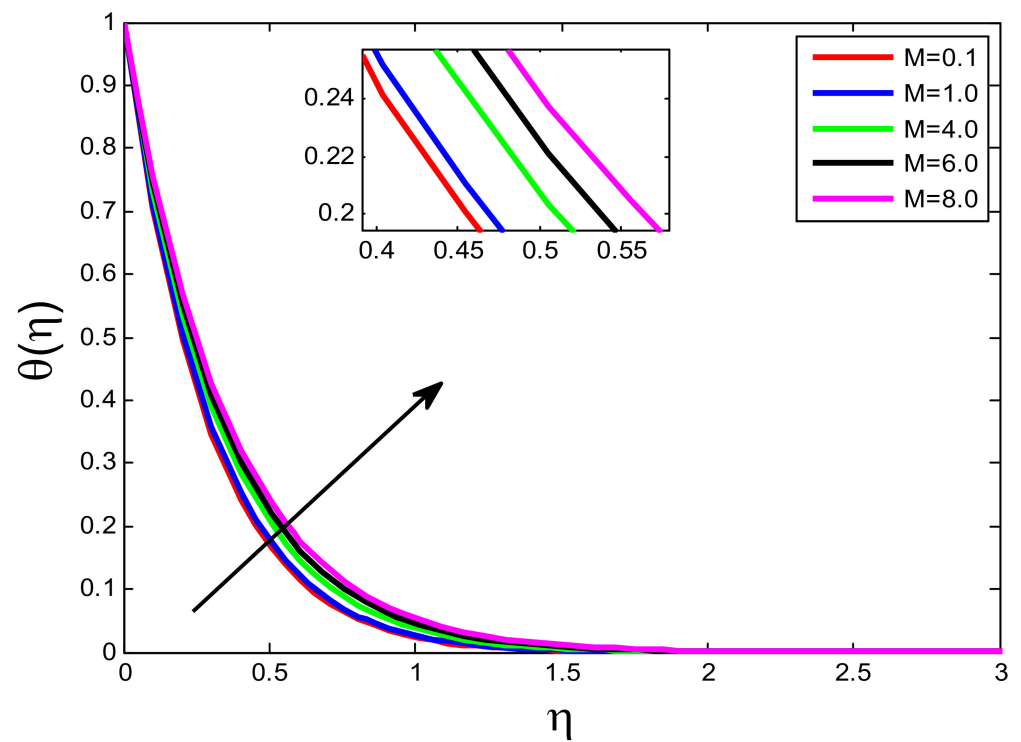


Figure 22. Influence of M on $\theta(\eta)$.

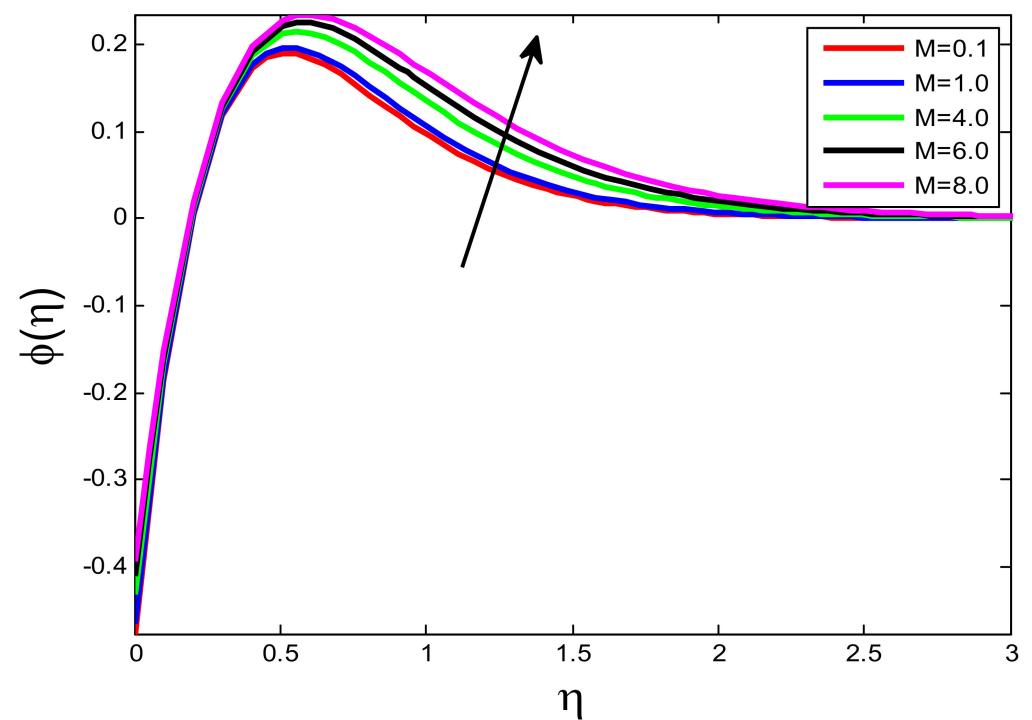


Figure 23. Influence of M on $\phi(\eta)$.

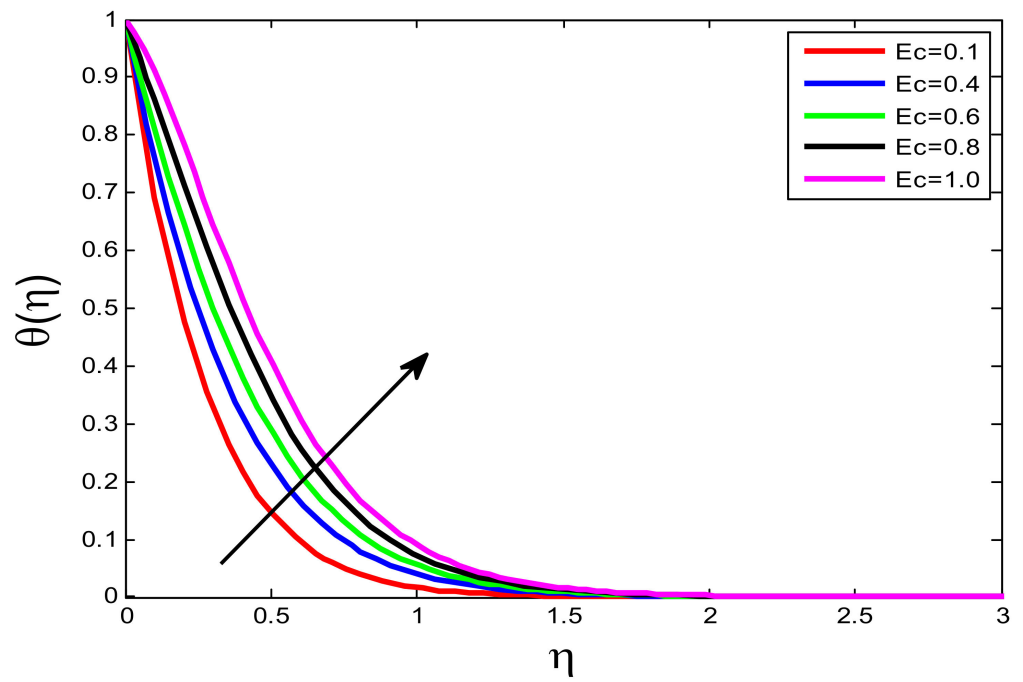


Figure 24. Influence of Ec on $\theta(\eta)$.

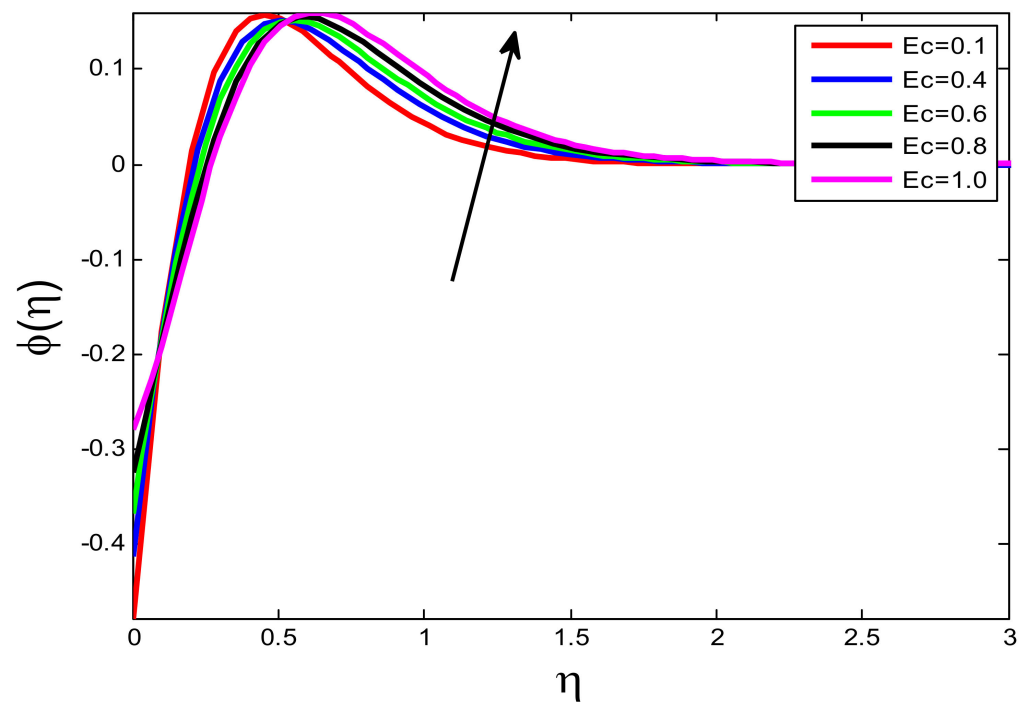


Figure 25. Influence of Ec on $\phi(\eta)$.

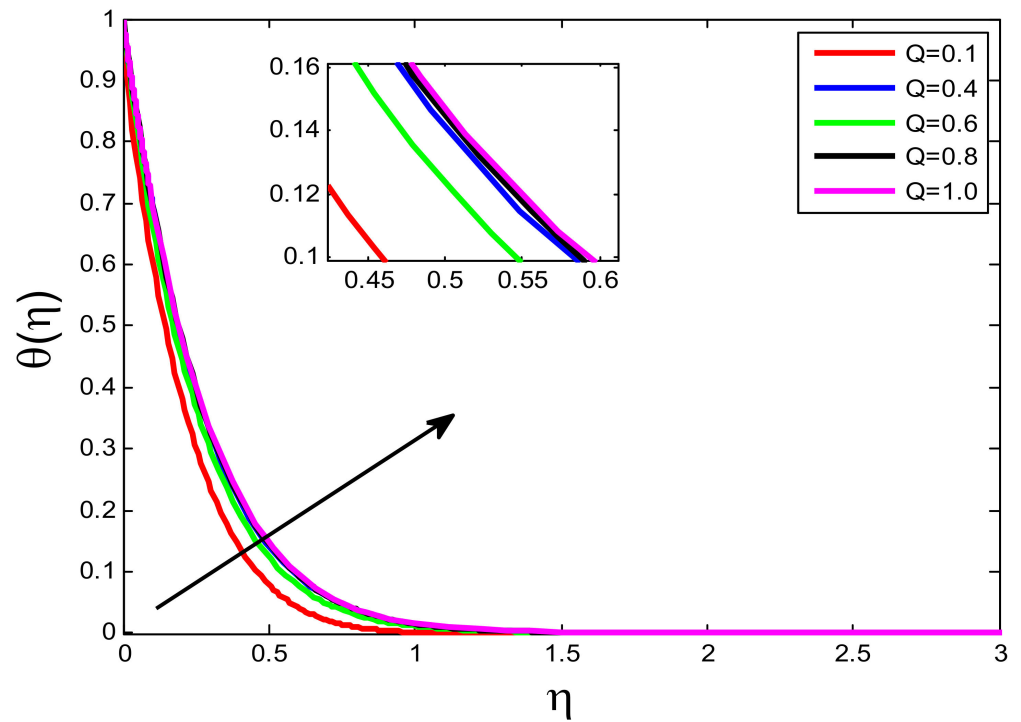


Figure 26. Influence of Q on $\theta(\eta)$.

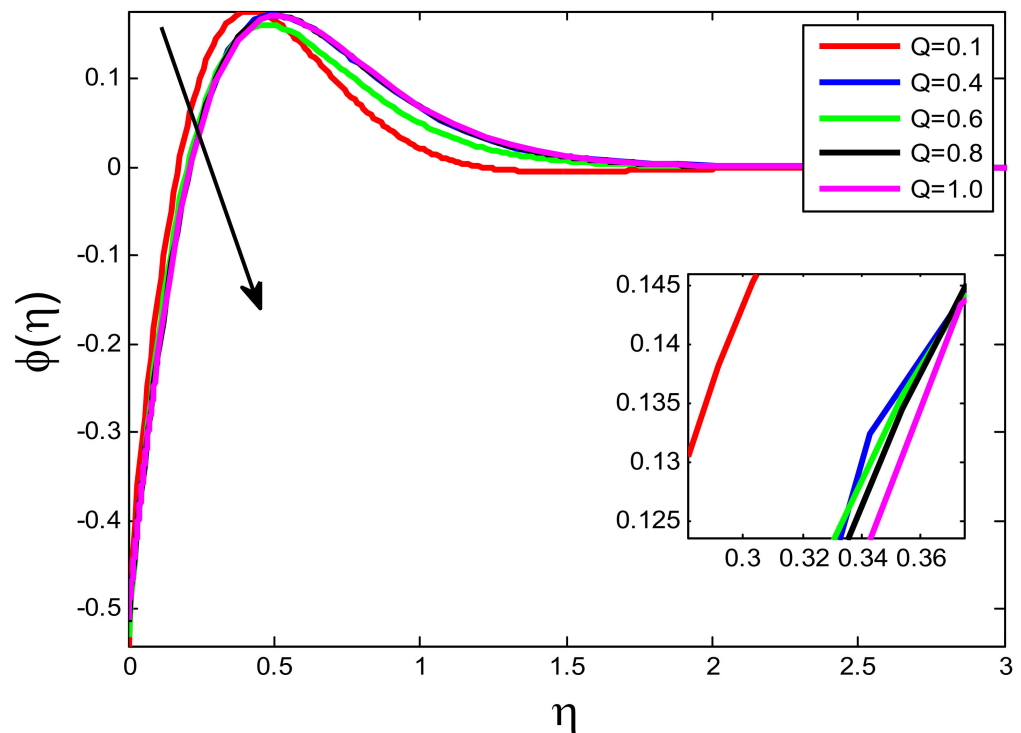


Figure 27. Influence of Q on $\phi(\eta)$.

4.2. Influence of Regulatory Flow Parameters on Skin Friction Coefficient $Re^{1/2}C_f$, Nusselt Number $Re^{-1/2}Nu$, and Sherwood Number $Re^{-1/2}Sh$

Figures 28–30 depict the action of Williamson fluid parameter W on the skin friction coefficient $Re^{1/2}C_f$, Nusselt number $Re^{-1/2}Nu$, and Sherwood number $Re^{-1/2}Sh$, respectively. The results indicate that with increasing increments of W $Re^{1/2}C_f$ and $Re^{-1/2}Sh$

increases but $Re^{-1/2}Nu$ is attenuated. The influence of Schmidt number Sc on skin friction coefficient $Re^{1/2}C_f$, Nusselt number $Re^{-1/2}Nu$, and Sherwood number $Re^{-1/2}Sh$ is illustrated in Figures 31–33. Graphs show that increasing Sc leads to decrease $Re^{1/2}C_f$, and $Re^{-1/2}Nu$ and increases $Re^{-1/2}Sh$. In Table 1, the present study is compared with the already published results for the validation of the current numerical solution. It is noted that there is good agreement between the current and existing results. Due to this strong agreement between the results, the validation of the current results is ensured.

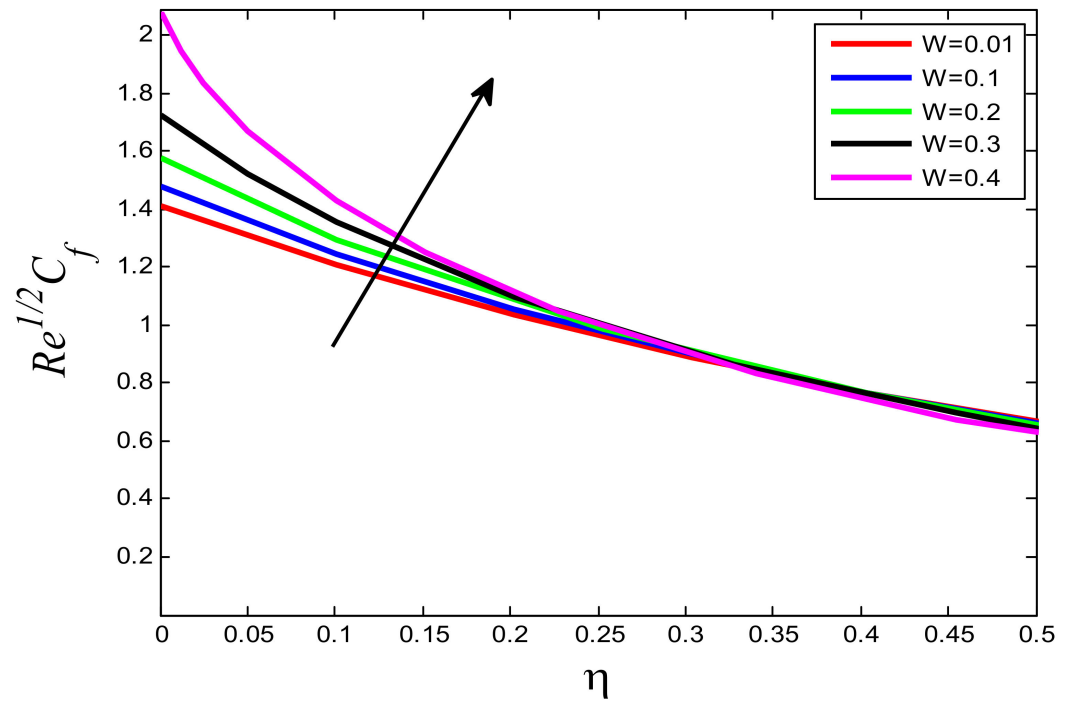


Figure 28. Influence of W on $Re^{1/2}C_f$.

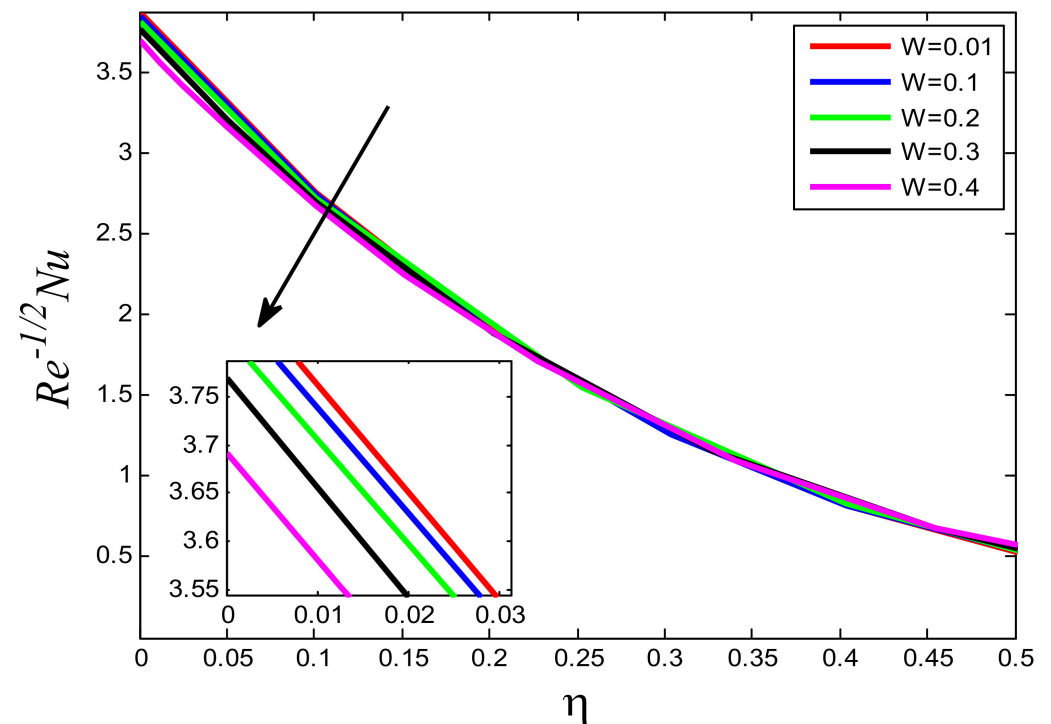


Figure 29. Influence of W on $Re^{-1/2}Nu$.

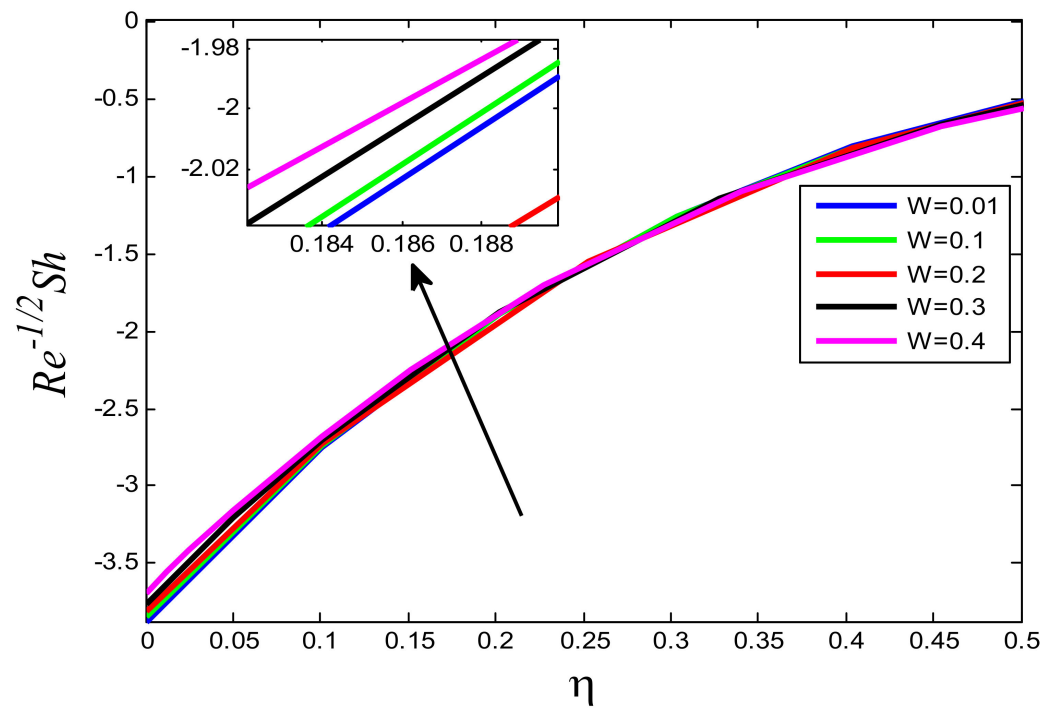


Figure 30. Influence of W on $Re^{-1/2}Sh$.

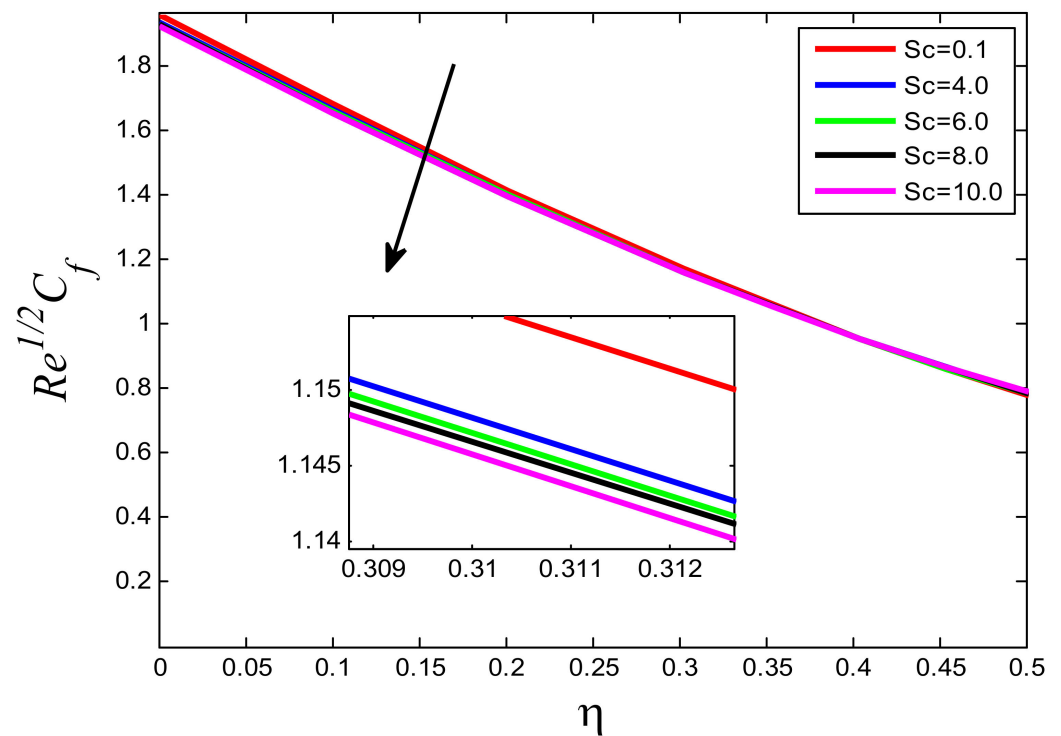


Figure 31. Influence of Sc on $Re^{1/2}C_f$.

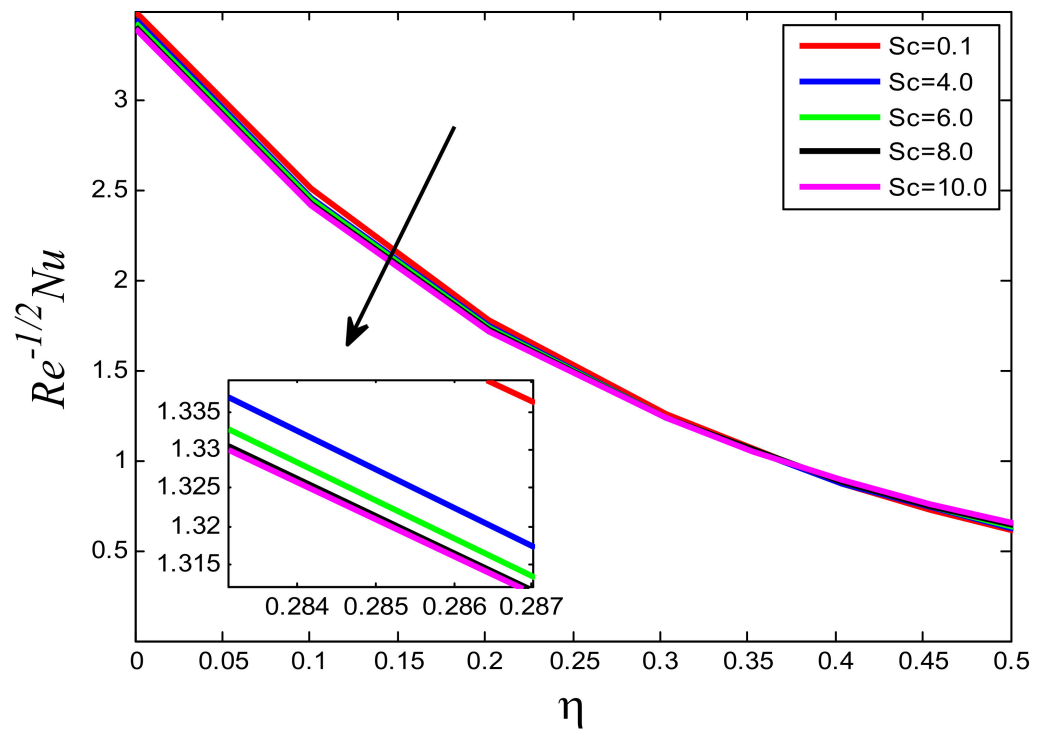


Figure 32. Influence of Sc on $Re^{-1/2}Nu$.

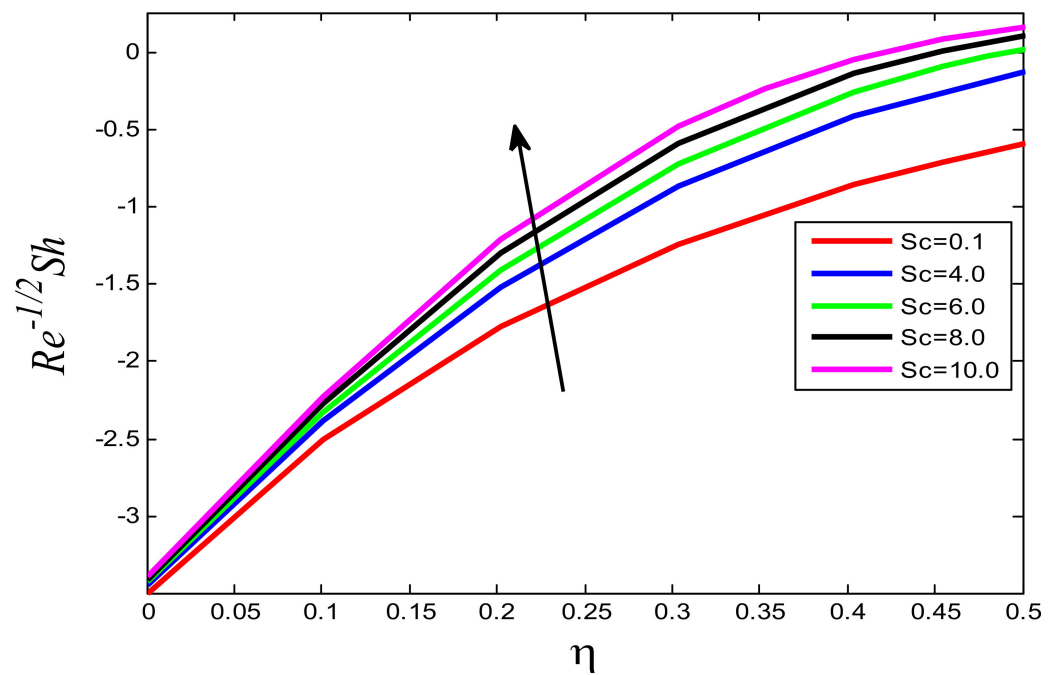


Figure 33. Influence of Sc on $Re^{-1/2}Sh$.

Table 1. Comparison of Nusselt number ($NuRe^{-1/2}$) for various values of Pr when $\lambda_T = \lambda_C = W = M = Nt = Nb = Ec = Q = Sc = 0$ and $n = 1$.

Pr	Gorla and Sidawi [37]	Megahed [38]	Present
0.07	0.06562	0.065531	0.065542
0.20	0.16912	0.169117	0.169128
2.0	0.91142	0.911358	0.911368
7.0	1.89546	1.895453	1.895462
20.0	3.35391	3.353902	3.353911

5. Conclusions

The current study deals with magnetohydrodynamic Williamson nanofluid flow and heat transfer past a non-linear stretching sheet fixed in a porous medium by incorporating heat generation and viscous dissipation influences. The transformed equation in forms of ODEs is solved with a bp4c solver and the results are shown in a graphical way. The main outcomes of the displayed results are summarized below:

- It is noted that increasing λ_T and Nb boosts $f'(\eta)$, but make weaker the increasing values of n , W , K , Pr , Nt , and M .
- The results show that there is an augmentation in $\theta(\eta)$ against increasing values of K , Nb , M , Ec , and Q but reverse scenario is seen for rising λ_T , n , Pr and Nt .
- It is noted that ϕ increases as W , K , Nb , M , and Ec increase, but the opposite trend is observed for augmenting λ_T , n , Nt , and Q .
- The graphical results indicate that $Re^{1/2}C_f$ increases for increasing W and decreases for increasing Sc .
- It has been viewed that enhancing W and Sc led to a decline in $Re^{-1/2}Nu$.
- It has been observed that $Re^{-1/2}Sh$ rises for increasing W and Sc .
- The present results are compared with existing results that show good agreement and endorse the validation of the current solution.

Author Contributions: Conceptualization, A.A. and A.A.; methodology, M.B.J.; software, A.S.A.; validation, A.A., A.S.A. and A.I.; formal analysis, A.S.A.; investigation, M.B.J.; resources, A.S.A.; data curation, A.I.; writing—original draft preparation, A.A.; writing—review and editing, A.A.; visualization, M.B.J.; supervision, A.S.A.; project administration, M.B.J.; funding acquisition, A.S.A. All authors have read and agreed to the published version of the manuscript.

Funding: This research was funded by [Imam Mohammad Ibn Saud Islamic University] grant number [RG-21-09-12]. The APC was funded by [Imam Mohammad Ibn Saud Islamic University].

Institutional Review Board Statement: Not applicable.

Informed Consent Statement: Not applicable.

Data Availability Statement: Data sharing is not applicable to this article as no new data were created or analyzed in this study.

Acknowledgments: The authors extend their appreciation to the Deanship of Scientific Research at Imam Mohammad Ibn Saud Islamic University for funding this work through Research Group no. RG-21-09-12.

Conflicts of Interest: The authors declare no conflict of interest.

References

1. Masuda, H.; Ebata, A.; Teramae, K. Alteration of Thermal Conductivity and Viscosity of Liquid by Dispersing Ultra-Fine Particles. Dispersion of Al_2O_3 , SiO_2 and TiO_2 Ultra-Fine Particles. *Netsu Bussei* **1993**, *7*, 227–233. [[CrossRef](#)]
2. Choi, S.U.; Eastman, J.A. *Enhancing Thermal Conductivity of Fluids with Nanoparticles*; Argonne National Lab.(ANL): Argonne, IL, USA, 1995; Volume 231, pp. 99–106.

3. Buongiorno, J.; Hu, W. Nanofluid coolants for advanced nuclear power plants. In Proceedings of the International Congress on Advances in Nuclear Power Plants 2005, Seoul, Korea, 15–19 May 2005; Volume 5, pp. 15–19.
4. Buongiorno, J. Convective Transport in Nanofluids. *J. Heat Transf.* **2006**, *128*, 240–250. [[CrossRef](#)]
5. Sheikholeslami, M.; Sadoughi, M.K. Simulation of CuO-water nanofluid heat transfer enhancement in presence of melting surface. *Int. J. Heat Mass Transf.* **2008**, *116*, 909–919. [[CrossRef](#)]
6. Abo-Dahab, S.M.; Abdelhafez, M.A.; Mebarek-Oudina, F.; Bilal, S.M. MHD Casson nanofluid flow over nonlinearly heated porous medium in presence of extending surface effect with suction/injection. *Indian J. Phys.* **2021**, *95*, 2703–2717. [[CrossRef](#)]
7. Shafiq, A.; Mebarek-Oudina, F.; Sindhu, T.N.; Abidi, A. A study of dual stratification on stagnation point Walters' B nanofluid flow via radiative Riga plate: A statistical approach. *Eur. Phys. J. Plus* **2021**, *136*, 407. [[CrossRef](#)]
8. Rasool, G.; Shafiq, A.; Alqarni, M.S.; Wakif, A.; Khan, I.; Bhutta, M.S. Numerical scrutinization of Dar-cy-Forchheimer relation in convective magnetohydrodynamic nanofluid flow bounded by nonlinear stretching surface in the perspective of heat and mass transfer. *Micromachines* **2021**, *12*, 374. [[CrossRef](#)]
9. Fares, R.; Mebarek-Oudina, F.; Aissa, A.; Bilal, S.M.; Öztop, H.F. Optimal entropy generation in Darcy-Forchheimer magnetized flow in a square enclosure filled with silver based water nanoliquid. *J. Therm. Anal. Calorim.* **2022**, *147*, 1571–1581. [[CrossRef](#)]
10. Shamshuddin, M.D.; Eid, M.R. Nth order reactive nanoliquid through convective elongated sheet under mixed convection flow with joule heating effects. *J. Therm. Anal. Calorim.* **2022**, *147*, 3853–3867. [[CrossRef](#)]
11. Ramesh, G.K.; Gireesha, B.J.; Gorla, R.S.R. Study on Sakiadis and Blasius flows of Williamson fluid with convective boundary condition. *Nonlinear Eng.* **2015**, *4*, 215–221. [[CrossRef](#)]
12. Nadeem, S.; Hussain, S.T.; Lee, C. Flow of a Williamson fluid over a stretching sheet. *Braz. J. Chem. Eng.* **2013**, *30*, 619–625. [[CrossRef](#)]
13. Nadeem, S.; Hussain, S.T. Heat transfer analysis of Williamson fluid over exponentially stretching surface. *Appl. Math. Mech.* **2014**, *35*, 489–502. [[CrossRef](#)]
14. Rashid, M.; Ansar, K.; Nadeem, S. Effects of induced magnetic field for peristaltic flow of Williamson fluid in a curved channel. *Phys. A Stat. Mech. Appl.* **2020**, *553*, 123979. [[CrossRef](#)]
15. Khan, N.A.; Khan, H. A boundary layer flows of non-Newtonian Williamson fluid. *Nonlinear Eng.* **2014**, *3*, 107–115. [[CrossRef](#)]
16. Salahuddin, T.; Malik, M.Y.; Hussain, A.; Bilal, S.; Awais, M. MHD flow of Cattaneo–Christov heat flux model for Williamson fluid over a stretching sheet with variable thickness: Using numerical approach. *J. Magn. Magn. Mater.* **2016**, *401*, 991–997. [[CrossRef](#)]
17. Raza, J.; Mebarek-Oudina, F.; Mahanthesh, B. Magnetohydrodynamic flow of nano Williamson fluid generated by stretching plate with multiple slips. *Multidiscip. Model. Mater. Struct.* **2019**, *15*, 871–894. [[CrossRef](#)]
18. Hamid, A.; Khan, M.; Khan, U. Thermal radiation effects on Williamson fluid flow due to an expanding/contracting cylinder with nanomaterials: Dual solutions. *Phys. Lett. A* **2018**, *382*, 1982–1991. [[CrossRef](#)]
19. Zehra, I.; Yousaf, M.M.; Nadeem, S. Numerical solutions of Williamson fluid with pressure dependent viscosity. *Results Phys.* **2015**, *5*, 20–25. [[CrossRef](#)]
20. Hayat, T.; Bibi, S.; Rafiq, M.; Alsaedi, A.; Abbasi, F. Effect of an inclined magnetic field on peristaltic flow of Williamson fluid in an inclined channel with convective conditions. *J. Magn. Magn. Mater.* **2016**, *401*, 733–745. [[CrossRef](#)]
21. Vafai, K.; Tien, C.L. Boundary and inertia effects on flow and heat transfer in porous media. *Int. J. Heat Mass Transf.* **1981**, *24*, 195–203. [[CrossRef](#)]
22. Jiang, P.-X.; Ren, Z.-P. Numerical investigation of forced convection heat transfer in porous media using a thermal non-equilibrium model. *Int. J. Heat Fluid Flow* **2001**, *22*, 102–110. [[CrossRef](#)]
23. Kothandapani, M.; Srinivas, S. On the influence of wall properties in the MHD peristaltic transport with heat transfer and porous medium. *Phys. Lett. A* **2008**, *372*, 4586–4591. [[CrossRef](#)]
24. Mahdi, R.A.; Mohammed, H.A.; Munisamy, K.M.; Saeid, N.H. Review of convection heat transfer and fluid flow in porous media with nanofluid. *Renew. Sustain. Energy Rev.* **2015**, *41*, 715–734. [[CrossRef](#)]
25. Gireesha, B.J.; Mahanthesh, B.; Manjunatha, P.T.; Gorla, R.S.R. Numerical solution for hydromagnetic boundary layer flow and heat transfer past a stretching surface embedded in non-Darcy porous medium with fluid-particle suspension. *J. Niger. Math. Soc.* **2015**, *34*, 267–285. [[CrossRef](#)]
26. Shehzad, S.A.; Abbasi, F.M.; Hayat, T.; Alsaedi, A. Cattaneo-Christov heat flux model for Darcy-Forchheimer flow of an Oldroyd-B fluid with variable conductivity and non-linear convection. *J. Mol. Liq.* **2016**, *224*, 274–278. [[CrossRef](#)]
27. Hosseinzadeh, K.; Gholinia, M.; Jafari, B.; Ghanbarpour, A.; Olfian, H.; Ganji, D.D. Nonlinear thermal radiation and chemical reaction effects on Maxwell fluid flow with convectively heated plate in a porous medium. *Heat Transf. Asian Res.* **2019**, *48*, 744–759. [[CrossRef](#)]
28. Abbas, A.; Shafqat, R.; Jeelani, M.B.; Alharthi, N.H. Significance of Chemical Reaction and Lorentz Force on Third-Grade Fluid Flow and Heat Transfer with Darcy–Forchheimer Law over an Inclined Exponentially Stretching Sheet Embedded in a Porous Medium. *Symmetry* **2022**, *14*, 779. [[CrossRef](#)]
29. Abbas, A.; Shafqat, R.; Jeelani, M.B.; Alharthi, N. Convective Heat and Mass Transfer in Third-Grade Fluid with Darcy–Forchheimer Relation in the Presence of Thermal-Diffusion and Diffusion-Thermo Effects over an Exponentially Inclined Stretching Sheet Surrounded by a Porous Medium: A CFD Study. *Processes* **2022**, *10*, 776. [[CrossRef](#)]

30. Abbas, A.; Jeelani, M.B.; Alharthi, N. Darcy–Forchheimer Relation Influence on MHD Dissipative Third-Grade Fluid Flow and Heat Transfer in Porous Medium with Joule Heating Effects: A Numerical Approach. *Processes* **2022**, *10*, 906. [[CrossRef](#)]
31. Mahanthesh, B.; Gireesha, B.J.; Gorla, R.S.R. Nonlinear radiative heat transfer in MHD three-dimensional flow of water based nanofluid over a non-linearly stretching sheet with convective boundary condition. *J. Niger. Math. Soc.* **2016**, *35*, 178–198. [[CrossRef](#)]
32. Seth, G.S.; Bhattacharyya, A.; Kumar, R.; Chamkha, A.J. Entropy generation in hydromagnetic nanofluid flow over a non-linear stretching sheet with Navier’s velocity slip and convective heat transfer. *Phys. Fluids* **2018**, *30*, 122003. [[CrossRef](#)]
33. Hayat, T.; Ullah, I.; Alsaedi, A.; Farooq, M. MHD flow of Powell-Eyring nanofluid over a non-linear stretching sheet with variable thickness. *Results Phys.* **2017**, *7*, 189–196. [[CrossRef](#)]
34. Seth, G.S.; Mishra, M.K. Analysis of transient flow of MHD nanofluid past a non-linear stretching sheet considering Navier’s slip boundary condition. *Adv. Powder Technol.* **2017**, *28*, 375–384. [[CrossRef](#)]
35. Jamshed, W.; Kumar, V.; Kumar, V. Computational examination of Casson nanofluid due to a non-linear stretching sheet subjected to particle shape factor: Tiwari and Das model. *Numer. Methods Partial. Differ. Equ.* **2020**, *38*, 848–875. [[CrossRef](#)]
36. Makinde, O.D.; Mabood, F.; Ibrahim, M.S. Chemically reacting on MHD boundary-layer flow of nanofluids over a non-linear stretching sheet with heat source/sink and thermal radiation. *Therm. Sci.* **2018**, *22*, 495–506. [[CrossRef](#)]
37. Reddy Gorla, R.S.; Sidawi, I. Free convection on a vertical stretching surface with suction and blowing. *Appl. Sci. Res.* **1994**, *52*, 247–257. [[CrossRef](#)]
38. Megahed, A.M. Williamson fluid flow due to a nonlinearly stretching sheet with viscous dissipation and thermal radiation. *J. Egypt. Math. Soc.* **2019**, *27*, 12. [[CrossRef](#)]
39. Qi, C.; Fan, F.; Pan, Y.; Liu, M.; Yan, Y. Effects of turbulator with round hole on the thermo-hydraulic performance of nanofluids in a triangle tube. *Int. J. Heat Mass Transf.* **2020**, *146*, 118897. [[CrossRef](#)]
40. Tang, J.; Qi, C.; Ding, Z.; Afrand, M.; Yan, Y. Thermo-hydraulic performance of nanofluids in a bionic heat sink. *Int. Commun. Heat Mass Transf.* **2021**, *127*, 105492. [[CrossRef](#)]
41. Kaood, A.; Hassan, M.A. Thermo-hydraulic performance of nanofluids flow in various internally corrugated tubes. *Chem. Eng. Process. Process Intensif.* **2020**, *154*, 108043. [[CrossRef](#)]
42. Zhai, X.; Qi, C.; Yang, Y.; Wang, J. Thermo-hydraulic performance of nanofluids under adjustable magnetic field. *Appl. Therm. Eng.* **2021**, *186*, 116491. [[CrossRef](#)]
43. Zhao, N.; Guo, L.; Qi, C.; Chen, T.; Cui, X. Experimental study on thermo-hydraulic performance of nanofluids in CPU heat sink with rectangular grooves and cylindrical bugles based on exergy efficiency. *Energy Convers. Manag.* **2019**, *181*, 235–246. [[CrossRef](#)]
44. Wang, G.; Qi, C.; Liu, M.; Li, C.; Yan, Y.; Liang, L. Effect of corrugation pitch on thermo-hydraulic performance of nanofluids in corrugated tubes of heat exchanger system based on exergy efficiency. *Energy Convers. Manag.* **2019**, *186*, 51–65. [[CrossRef](#)]
45. Qi, C.; Hu, J.; Liu, M.; Guo, L.; Rao, Z. Experimental study on thermo-hydraulic performances of CPU cooled by nanofluids. *Energy Convers. Manag.* **2017**, *153*, 557–565. [[CrossRef](#)]
46. Avramenko, A.A.; Kobzar, S.G.; Shevchuk, I.V.; Kuznetsov, A.V.; Iwanisov, L.T. Symmetry of turbulent boundary-layer flows: Investigation of different eddy viscosity models. *Acta Mech.* **2001**, *151*, 1–14. [[CrossRef](#)]
47. Avramenko, A.A.; Shevchuk, I.V. *Modelling of Convective Heat and Mass Transfer in Nanofluids with and without Boiling and Condensation*; Springer Nature: London, UK, 2022.